Analysis of LITTLE NUCLEI family regulating nuclear morphology in *Arabidopsis thaliana*

シロイヌナズナにおける細胞核形態を制御する LITTLE NUCLEI ファミリーの解析

Yuki Sakamoto

Department of Biological Science, Graduate School of Science, Osaka University

Dec. 2013

Contents

Abbreviations

A. thaliana, *Arabidopsis thaliana*
ATP, Adenosine-5'-triphosphate
BDM, 2,3-Butanedione monoxime
B. stricta, Barbarea stricta
CaMV, Cauliflower mosaic virus
DAG, Day after germination
DAPI, 2-(4-amidinophenyl)-1H -indole-6-carboxamidine
D. carota L., *Daucus carota* L.
DIG, Digoxigenin
DMSO, Dimethyl sulfoxide
DTT, Dithiothreitol
EGTA, Ethylene glycol tetraacetic acid
FISH, Fluorescence *in situ* hybridization
GFP, Green fluorescent protein
GM, Germination
GUS, β -glucuronidase
KASH, Klarsicht/ANC-1/Syne homology protein
LBR, Lamin B receptor
LC-MS/MS, Liquid chromatography tandem mass spectroscopy
LEM, Lap-Emerin-Man
LINC, LITTLE NUCLEI
MES, 2-(N-morpholino)ethanesulfonic acid
MS, Murashige and Skoog
N. benthamiana, Nicotiana benthamiana
NMCP, Nuclear matrix constituent protein
Nup, Nucleoporin
PAGE, Poly-acrylamide gel electrophoresis
PIPES, Piperazine-N,N'-bis(2-ethanesulfonic acid)
rDNA, ribosomal DNA
rhl, root hairless
RT-PCR, Reverse transcription polymerase chain reaction
SDS, Sodium dodecyl sulfate
SUN, Sad1/UNC84 domain protein
T-DNA, Transfer DNA
WIP, WPP domain-interacting proteins
WIT, WPP domain–interacting tail-anchored proteins
X-Gluc, 5-Bromo-4-chloro-1H-indol-3-yl β-D-glucopyranosiduronic acid
YFP, Yellow fluorescent protein

Abstract

The morphology of plant nuclei varies among different species, organs, tissues, and cell types. There is a fixed relationship between nuclear volume and DNA content; a large nucleus contains a large amount of DNA. However, mechanisms and factors involved in the regulation of nuclear morphology are poorly understood.

In this thesis, in chapter 1, I first revealed that treatments of *Arabidopsis thaliana* leaves and isolated nuclei with actin- and microtubule- depolymerizing reagents did not induce any nuclear morphological change, which suggested that cytoskeletons are not involved in the maintenance of nuclear morphology. To find intranuclear factors involved in the regulation of nuclear morphology, I prepared a crude nuclear lamina fraction from the demembranated nuclei. A total of 660 proteins were identified as putative nuclear lamina proteins by Liquid chromatography tandem mass spectroscopy (LC-MS/MS) of the fraction and I selected 63 of the 660 proteins harboring putative DNA-binding motifs or with unknown functions. Among their T-DNA insertion lines, nuclei of *little nuclei1* (*linc1*) and *linc4* disruptants were more spherical than those of wild-type plants. Most of the land plants harbor *LINC* homologues and *A. thaliana* harbors four *LINC* genes. LINC1, LINC2, and LINC3 belong to the one type, while LINC4 belongs to the other type.

In chapter 2, I investigated expression patterns of LINC1-LINC3 fused with β-glucuronidase (GUS) and expressed under the control of individual native promoter in wild-type plants. LINC1-LINC3 were mainly expressed in immature tissues and their expression levels became lower with tissue maturation. Further, I investigated the intracellular localization patterns of LINC1-LINC4 fused with GFP or YFP expressed under the control of the cauliflower mosaic virus (CaMV) 35S promoter or individual native promoters in the wild-type plants and *linc* disruptants. In interphase cells, LINC1-LINC4 were mainly localized at nuclear periphery. In mitotic cells, LINC1 seemed to be

localized on the condensing chromatin during prometaphase to anaphase, whereas other LINCs were localized diffusely in the cytoplasm.

In chapter 3, I analyzed phenotypes of the *linc* disruptants. *linc1-linc4* single disruptants and *linc1/linc4* and *linc2/linc3* double disruptants were prepared. The disruptants exhibited normal growth under the present experimental conditions. First, nuclear morphology was semi-quantified in leaf and root epidermal cells. *linc1, linc4,* and *linc1/linc4* disruptants exhibited extremely spherical and small nuclei, and *linc2, linc3,* and *linc2/linc3* disruptants exhibited moderately spherical nuclei. Consequently, LINC1 and LINC4 functioned predominantly and LINC2 and LINC3 subordinately in the regulation of nuclear morphology in leaf and root epidermal cells. Although the nuclear morphology in these *linc* disruptants was more or less abnormal, all *linc* disruptants exhibited almost normal light-dependent nuclear movement and DNA content compared with the wild-type plants. Furthermore, the chromatin architecture in *linc1/linc4* disruptants was investigated by fluorescence *in situ* hybridization (FISH). The number of signals of centromere and 45S-rDNA recognizing probes in *linc1/linc4* disruptants were significantly lower than that in wild-type plants. In summary, I clarified that LINC1 and LINC4 localized at nuclear periphery play predominant roles in regulation of nuclear morphology and chromatin architecture without affecting the DNA content.

Introduction

Nuclear compartment

Living things have the ability of self-replication. Parents hand down information specifying the characteristics that their offspring shall have. On the earth, living things have the genetic information in DNA and some of them acquired a special compartment to store DNA in each cell. Robert Brown found this large compartment and named NUCLEUS (nucleus means almond in Latin) in 1831, although Leeuwenhoek and Franz Bauer had already suggested the exitance of such compartment before his discovery. Today, it is known that almost eukaryotic cells contain one nucleus, while exceptionally, for example, a red blood cell and xylem cell do not contain the nucleus, and a skeletal muscle cell, some of the green algae and fungi contain multiple nuclei. Although nucleus is one of the largest organelle in eukaryotic cell except for plant vacuole, DNA is very tightly packed into it. In the case of human, about 2 meters of DNA is contained in each nucleus whose diameter is about 6 μm, which is geometrically equivalent to packing 40 km of extremely fine thread into a tennis ball. Strangely, this extremely tight packing, achieved by a lot of DNA binding proteins such as histone, allows a variety of intranuclear enzymes to easily work for replication, transcription, and restoration. The seemingly contradictory tight-packing structure and flexible enzyme activities were based on strategically constructed nuclear and chromatic architecture.

Nucleus is divided from cytoplasm by a nuclear envelope formed by two lipid bilayer membranes; inner nuclear envelope and outer nuclear envelope. Inner nuclear envelope contains membrane proteins interacting with nuclear lamina and chromatin, outer nuclear envelope contains membrane proteins interacting with cytoplasmic proteins. Nuclear lamina forms a thin sheet-like meshwork inside the nucleus, just beneath the inner nuclear envelope. Nuclear envelope is perforated by large nuclear pores, which transport molecules between the nucleus and cytoplasm. The nucleus

has several nucleoli where ribosome is synthesized in nucleoplasm. The functions of these nuclear components have been extensively studied by a lot of researchers but only a few scientists as me have been interested in the shape and morphology of nucleus.

In the nucleus, DNA is divided into multiple chromosomes, for example, a human genome is in 24 chromosomes and an *A. thaliana* genome is in 5 chromosomes. In the interphase nucleus, each chromosome occupies specific territory and is never randomly distributed. This chromosome distribution patterns in the nucleus are involved in the epigenetic regulation of gene expression. For example, the chromosome high gene density and high gene transcription activity such as 19th chromosome of human is localized at the central part of nucleus, whereas the chromosome low gene density such as 18th chromosome of human are localized at perinuclear region (Cremer and Cremer, 2001). Additionally, the centromeres and telomeres also exhibit characteristic distribution patterns in the nucleus. Although the information of chromosome distribution patterns in interphase seemingly disappears at the time of cell division, similar distribution patterns reappear in the daughter cells (Gerlich et al., 2003). The chromatin and chromosome distribution patterns are positively regulated and affect gene expression.

Nuclear morphology in animal cells

The nucleus of animal cells is typically spherical or ellipsoidal, but some specialized cells undergo dramatic changes in nuclear shape during differentiation and maturation. For example, spermatids have extremely elongated nuclei (Burgos and Fawcett, 1956; Tokuyasu, 1974; Dadoune, 1995), and neutrophils develop extremely lobulated nuclei (Hoffmann et al., 2007). The nuclear morphology is determined through interactions between intranuclear and extranuclear factors. In animal cells, nuclear lamins and nuclear envelope proteins composing the SUN-KASH complex play indispensable roles in the regulation of nuclear morphology. Lamins are main components of the

nuclear lamina and are directly associated with Sad1/UNC84 domain proteins (SUNs) of the SUN-KASH complex (Starr and Fridolfsson, 2010). SUNs traversing the inner nuclear envelope interact with Klarsicht/ANC-1/Syne homology proteins (KASHs) traversing the outer nuclear envelope (Starr and Fridolfsson, 2010). Disruption or mutation of any of the *lamin* or *KASH* genes induces abnormal nuclear morphology (Sullivan et al., 1999; Shimi et al., 2010; Lüke et al., 2008; Khatau et al., 2009). In contrast, nuclear morphology is affected by the extranuclear cytoskeleton. Cytoplasmic actin filaments, microtubules, and intermediate filaments are associated with the outer nuclear envelope KASHs (Starr and Fridolfsson, 2010). In mouse embryonic fibroblasts, thick bundles of actin filaments are organized into a cap structure above the nucleus. Treatment with latrunculin B, which disrupts the actin cap structure, leads to almost complete abrogation of the regulation of nuclear morphology (Khatau et al., 2009). Addition of retinoic acid to leukemic HL-60 cells changes nuclear morphology from an ovoid to a lobulated shape. Nocodazole treatment prevents nuclear lobulation in response to retinoic acid treatment, whereas taxol treatment induces lobulation without retinoic acid (Olins and Olins, 2004). Taken together, the functional association of cytoskeletons with KASH-SUN-lamins is critical to transmit the extranuclear force to the intranuclear lamins in order to regulate nuclear morphology (Starr and Fridolfsson, 2010).

Since late 19th century, it has been recognized that human neutrophil contain non-ovoid, lobulated (segmented) nucleus. The neutrophil nucleus typically has three lobes, but this varies from two to five, and lobes are connected by thin strands of chromatin. Pelger-Huet anomaly is known to exhibit an autosomal dominant inherited abnormality of neutrophils nucleus, characterized by reduced nuclear segmentation and an apparently looser chromatin structure. Heterozygous state generates benign state with altered nucleus, however, homozygous state generates mental retardation and skeletal defects with ovoid nucleus. In 21th century, it is elucidated that Pelger-Huet anomaly is caused by mutation in lamin B receptor (LBR) gene (Hoffmann et al., 2002). LBR is an integral inner nuclear

envelope protein which interacts with lamin B. These studies suggest that defect of the factors involved in regulation of nuclear morphology and chromatin structure induces hereditary disease.

Nuclear morphology in plant cells

In plants, nuclei from different cell types exhibit different shapes, volume, structure (Bennett, 1984), organization of chromatin (Manuelidis and Borden, 1988), and distribution of nuclear proteins (Zirbel et al*.,* 1993). For example, in the several species of moss, spherical nuclei are contained in chloronemal cells, spindle shaped nuclei are in matured caulonemal cells and food-conducting cells, and spirally-coiled rods nuclei are in the spermatozoid (Paolillo et al., 1968ab; Ligrone and Dukett, 1994; Duckett and Ligrone, 1995; Pressel et al., 2008). In angiosperms *Triticum aestiyum*, antipodal cell nuclei, containing polytenized chromosomes, are sub-spherical and often have a highly convoluted nuclear envelope, while mature sperm nuclei are haploid and elongated with a smooth profile (Bennett, 1984).

Recently, it becomes possible to observe nuclei in living tissues by using fluorescent markers in *Arabidopsis thaliana*. Chytilova et al. (1999) succeeded in transgenic expression of green fluorescent protein (GFP) fused with nuclear localization signal and to β-glucuronidase (GUS). The nuclear localization signal sequence induces migration of the protein into the nucleus and the GUS sequence increases the size of protein such that it is prevented from passive movement across the nuclear pores. Taking advantage of this technique, Chytilova et al. (1999) examined correlation between nuclear morphology and cell shape. In isodiametric cells, nuclei are generally spherical, while in cylindrical or highly elongated cells, nuclei are ellipsoidal or elongated shape. For example, the shape of root tip cells is square and they contain small spherical nuclei. In contrast, within the root elongation zone, there are rectangular epidermal and cortical cells, which contain ellipsoidal or fusiform-shaped nuclei. Within root vascular tissues, nuclei are generally cylindrical, and within root

hair cells, nuclei are fusiform-shaped and often form subnuclear blebs connected by thin threads of nucleoplasm. The similar variations in nuclear shape are also seen in aerial tissues.

It may be possible to imagine that the morphological variations of nucleus are advantageous to cell functions; the small size of the sperm nuclei might contribute to its smooth transportation in a pollen tube in angiosperms or swimming towards the archegonium in bryophytes and pteridophytes, while the large size of the antipodal nucleus might contribute to its high transcriptional activity. However, I have not yet seen direct evidences for such biological significance of morphological variations of nucleus.

Nuclear morphology and ploidy level in plant cells

In the bryoid moss *Polytrichum juniperinum*, food-conducting cells in both the gametophyte and sporophyte contain highly elongated nuclei more than 15 μm in length and 5 μm in width (Ligrone and Duckett, 1994), while the spermatozoid nuclei are spirally-coiled rods less than 0.2 μm in diameter with completely condensed chromatin (Paolillo et al., 1968ab). In several species of the bryoid mosses, during differentiation of caulonemal and rhizoid cells, the nuclear shape changes from spherical and ovoid to highly elongated and spindle-shaped. In caulonemal cells, there are positive relations between the amount of DNA in nucleus and the volume, length, and shape parameter (length/width) of nucleus (Kingham et al., 1995). Therefore the morphological variety of nucleus may reflect endoreduplication.

Two highly endopolyploid species, *A. thaliana* and *Barbarea stricta*, exhibit a highly positive correlation between nuclear volume and DNA content (Jovtchev et al., 2006), whereas nuclei of the *root hairless 1* mutant (rhl1) of *A. thaliana* are smaller than those of the wild-type plants. The *rhl1* cells undergo only the first two rounds of endoreduplication and stall at 8C, whereas the wild-type cells usually reach 32C (Sugimoto-Shirasu et al., 2005). Moreover, a correlation between nuclear

volume and genome size has been demonstrated by examining 2C nuclei isolated from more than 10 plant species (Fujimoto et al., 2005; Jovtchev et al., 2006). Taken together, these results suggest that there is a fixed relationship between nuclear volume and DNA content. In addition, a positive correlation between DNA content or ploidy level and cell volume was reported in several plant species (Jovtchev et al., 2006), which further suggests that nuclear volume correlate with cell volume. However, it has not been revealed whether regulatory mechanisms for DNA content, nuclear volume, and cell volume are separate. In addition, the shape of nuclei in *A. thaliana* is not similar to that in *B. stricta,* although their DNA contents and ploidy levels are similar.

Nuclear morphology regulated by cytoskeletons in plant cells

In electron microscopy of food-conducting cells of the moss *Mnium hornum*, elongated nuclei are associated with cytoplasmic microtubules, and the both poles of nuclear envelope forms long tubule like structures that extend towards the distal ends of the cells (Ligrone and Dukett 1994). A microtubule-depolymerizing reagent oryzalin but not an actin-depolymerizing reagent cytochalasin induced changes in the elongated nuclear shape in differentiated caulonemal, rhizoid, and food-conducting cells (Pressel et al., 2008). These studies suggested that microtubule cytoskeleton is responsible for nuclear shaping in the moss one of the base land plants. In pollen tubes of angiosperms, the vegetative nucleus takes elongated morphology. By treating germinating pollen with an actin-depolymerizing reagent cytochalasin D, the morphology of vegetative nucleus became much more spherical (Heslop-Harrison and Heslop-Harrison, 1989). Additionally, in the case of sperm nuclei in *Cyrtanthus mackenii* pollen tubes, the shape of two sperm nuclei is not same. After treatment with oryzalin differences in nuclear shape between the two sperm nuclei disappeared (Hirano and Hoshino, 2010). Taken together, cytoskeleton-mediated forces may contribute to maintain the nuclear shape in plant cells. However, this was not the case of root hair cells treated with actin- or

microtubule-depolymerizing reagents (Chytilova et al., 2000), suggesting the existence of cell-type specific regulation for the maintenance of nuclear morphology.

Molecules involved in regulation of plant nuclear morphology

Plants do not contain lamin homologs, and only a few plant nuclear lamina proteins have been characterized to date (Mcnulty and Saunders, 1992; Gindullis et al., 1999; Yu and Moreno Díaz de la Espina, 1999; Rose et al., 2003). One such protein is nuclear matrix constituent protein 1 (NMCP1), which has been identified in embryogenic *Daucus carota* L. cells (Masuda et al., 1997). NMCP1 contains extensive coiled-coil domains and is localized to the nuclear lamina as animal lamin (Masuda et al., 1997). LITTLE NUCLEI1–4 (LINC1–4), which contains sequences homologous to NMCPs, extensive coiled-coil domains, and nuclear localization signals have been identified in *A. thaliana* (Dittmer et al., 2007; Meier, 2007; Ciska et al., 2013). LINC1 and LINC2 are localized to the nuclear periphery and nucleoplasm, respectively. Nuclei of disruptants of one of these genes are more spherical and smaller than those of the wild-type plants. LINC1 and LINC2 double disruption results in a synergistic decrease in nuclear size and synthetic whole-plant dwarfing phenotype, suggesting a functional redundancy among LINC1 and LINC2 (Dittmer et al., 2007). The nuclear envelope complex is composed of SUNs and WPP domain-interacting proteins (WIP), which are the first identified plant KASHs and are necessary for the maintenance of nuclear morphology in *A. thaliana* (Xu et al., 2007; Oda and Fukuda, 2011; Zhou et al., 2012). More recently, some of myosin XI mutants were reported to exhibit abnormal nuclear morphology (Ojangu et al., 2012; Tamura et al., 2013). Especially, myosin XI-I can interact indirectly with WIP through the direct binding to WPP domain–interacting tail-anchored proteins (WIT), which is localized at the outer nuclear envelope and can bind directly to WIP (Zhao et al., 2008; Tamura et al., 2013). However, how the nuclear lamina proteins, SUN-KASH complex, and cytoskeletons function and whether other protein factors are

involved in the maintenance of plant nuclear morphology remain to be elucidated.

Nuclear positioning and movement

In moss chloronemata, the apical cell and its derivatives have a centrally located nucleus. The nucleus maintains a constant distance from the growing apical tip. In angiosperms, the vegetative nucleus passes into the growing pollen tube and maintains a constant distance from the growing apical tip. As mentioned above, the shape of vegetative nucleus is maintained by actin filaments (Heslop-Harrison and Heslop-Harrison, 1989). The migration of vegetative nucleus is also mediated by actin filaments, supported by the inhibitory effects of cytochalasin D on pollen tube growth and vegetative nucleus migration (Heslop-Harrison and Heslop-Harrison, 1989). Characteristic nuclear movements can be seen in root hairs with their growth. In growing root hairs, the nucleus migrates at close distance form the apical tip. After the root hair stops growing, the nucleus gets out from the sub-apical tip region and migrates randomly throughout the root hair in both directions. Actin filaments are necessary for the uni-directional movement and positioning of the nucleus at the apex during growth and also for the bi-directional movement in mature root hairs (Chytilova et al., 2000; Ketelaar et al., 2002). In *A. thaliana* leaf cells, nuclei show a unique movement in response to environmental light (Iwabuchi et al. 2007). Under dark condition, nuclei are positioned at the center of the bottom of cells, whereas after irradiation with strong blue light, nuclei migrate to anticlinal walls. This migration is inhibited by actin-depolymerizing regent latrunculin B but not microtubule-depolymerizing regent propyzamide (Iwabuchi et al. 2010). Therefore, plant nuclear movements mainly depend on actin cytoskeleton although there are a few reports suggesting an involvement of microtubules (Astrom et al., 1995; Sieberer et al., 2002).

Overview

In this study, I used in *A. thaliana* leaves cytoskeleton inhibitors to demonstrate that cytoskeletons are not involved in the maintenance of nuclear morphology. Next, in order to identify novel proteins involved in the regulation of nuclear morphology, I isolated a crude nuclear lamina fraction from *A. thaliana* leaves and identified LINC1 and LINC4 form that fraction. I investigated expression patterns and intracellular localization patterns of LINCs and phenotypes of linc disruptants. It is suggested that LINCs play important roles in the regulation of nuclear morphology.

Materials and Methods

Plant materials and growth conditions

A. thaliana ecotype Col-0 was used as the wild-type plant. I used the following *A. thaliana LINC* disruptants: *linc1* (SALK_016800), *linc2* (SALK_0766530), *linc3* (SALK_099283), and *linc4* (SALK_079288). These *linc* disruptants were crossed to produce *linc1/linc4* and *linc2/linc3* double disruptants. Seeds were surface sterilized with 70% (v/v) ethanol and then sown onto GM medium [MS salts, 1% (w/v) sucrose, 0.4% (w/v) gellan gum, and 0.05% (w/v) MES-KOH at pH 5.7]. The seeds were incubated at 4°C for 1 day to break seed dormancy and then grown at 22°C for 7 days under long-day conditions (16 h light, 70 μmol m^{-2} s^{-1}: 8 h dark). The plants were transferred to soil for subsequent growth.

Genotyping of individual T-DNA alleles was performed by standard PCR using the allele-specific primers as follows: for *linc1* (SALK_016800), LP, 5′-CTCCTCCGGTGACACTATCTG-3′ and RP, 5′-AAAAGAAAGGGAGTTGCAAGC-3′; for *linc2* (SALK_0766530), LP, 5′- CTCGAACTGAGCCATTCTGTC-3′ and RP, 5′-AGCTCATTGCTAGAGAAGGGG-3′; for *linc3* (SALK_099283), LP, 5′-TTGCCTCTGAAATTCCATGTC-3′ and RP, 5′-CAGTGACGCATATACGCATTC-3′; and for *linc4* (SALK_079288), LP, 5′-CAACTTGGAGATTGCGTTAGC-3′ and RP, 5′-CACGCTGTATCTTGCTAAGCC-3′ in combination with the T-DNA-specific primer LBa1, 5′-TGGTTCACGTAGTGGGCCATCG-3′.

Hoechst staining and semi-quantitative nuclear morphology analysis

Sample leaves were fixed in 2% (w/v) formaldehyde, freshly prepared from paraformaldehyde, and 0.3% (w/v) glutaraldehyde in a PIPES buffer (10 mM EGTA, 5 mM $MgSO_4$,

and 50 mM PIPES at pH 7.0) for 2 h with evacuation for the first 5 min. The leaves were stained with a Hoechst solution (5 μg/ml Hoechst 33342 (Calbiochem, Darmstadt, Germany) in the PIPES buffer) containing 0.03% (v/v) Triton X-100 for 1 h and then with the Hoechst solution overnight when needed. Sample roots were fixed in 4% (w/v) formaldehyde, freshly prepared from paraformaldehyde, in the PIPES buffer for 1 h. Fixed roots were treated with 0.5% (w/v) Cellulase Onozuka RS and 0.05% (w/v) Pectolyase Y-23 in the PIPES buffer for 5 min at 37°C and then stained with the Hoechst solution for 10 min. Samples were observed using a DeltaVision microscope with an Olympus IX70 stand (Personal DV; Applied Precision, Issaquah, Washington, USA). Image processing programs (Photoshop 6.0; Adobe Systems, San Jose, California, USA; ImageJ 1.45q; National Institutes of Health, Bethesda, Maryland, USA) were used to analyze the nuclear circularity index and nuclear area. The circularity index was calculated using the equation $4\pi A/P^2$ where A is area and P is perimeter. The index indicates how closely each nucleus corresponds to a spherical shape; a perfect sphere has a value of 1.

When the effects of cytoskeletal and myosin inhibitors on the nuclear morphology were examined, sample leaves after evacuation in the PIPES buffer for 5 min or demembranated nuclei were further treated with 10 μM latrunculin B (Calbiochem) and/or 100 μM propyzamide (Wako, Osaka, Japan) or 100 μM BDM in the PIPES buffer for 1 h. Under these conditions, actin and microtubule cytoskeletons were almost completely disrupted, respectively (Iwabuchi et al. 2010). Stock solutions of inhibitors were prepared in dimethyl sulfoxide (DMSO) and diluted to the final concentration with deionized water at use. Control leaves were treated with 1% DMSO. After inhibitor treatments, sample leaves were fixed and stained as mentioned above. Demembranated nuclei were stained by the Hoechst solution for 5 min without fixation.

Preparation of demembranated nuclei and crude nuclear lamina fraction

Whole plants were maintained in darkness for 36 h to consume starch grains in chloroplasts that were contaminated in the demembranated nuclei fraction. Leaves were treated with an enzyme solution composed of 1% (w/v) Cellulase Onozuka RS (Yakult Pharmaceutical, Tokyo, Japan), 0.1% (w/v) Pectolyase Y-23 (Kyowa Chemical, Kagawa, Japan), 0.6 M mannitol, 80 mM $MgCl_2$, and 20 mM MES at pH 5.7 for 2 h at 25°C. Protoplasts were filtered through 50-μm mesh, suspended in nuclear isolation (NI) buffer [10 mM $MgCl_2$, 10 mM KCl, 0.4 M sucrose, 0.5% (v/v) Triton X-100, 10 μM DTT, 1 tablet per 50 ml Complete Protease Inhibitor Cocktail (Roche, Basel, Switzerland), and 10 mM PIPES at pH7.0], and then incubated with gentle shaking for 30 min at 4°C. After centrifugation at 1000 ×*g* for 5 min, the pellet was suspended in NI buffer, and the same incubation and centrifugation cycles were repeated. The resultant pellet was designated as a demembranated nuclei fraction. The fraction was further treated with 100 μg/ml DNase and 100 μg/ml RNase in NI buffer without Triton X-100 for 1 h at 25°C. After centrifugation at 10,000 ×*g* for 5 min, the pellet was washed twice with NI buffer without Triton X-100. The crude nuclear lamina fraction was usually prepared from 5 g leaves.

Electron microscopy

The crude nuclear lamina fraction was put on Cu meshes coated by formvar and poly-L-lysine and observed after negative staining with 1% (w/v) uranyl acetate using a transmission electron microscope (JEOL 1200 EX; JEOL, Tokyo, Japan) at 80 kV.

Mass spectrometric analysis

The crude nuclear lamina fraction was subjected to sodium dodecyl sulfate-polyacrylamide gel electrophoresis followed by Flamingo staining (Bio-Rad, Hercules, California, USA). The stained gel was cut into 16 sections, and the gels were washed with 100% acetonitrile and dried in a vacuum

concentrator (Fujiwara et al., 2009). The dried gels were treated with reduction solution (10 mM DTT, 50 mM ammonium bicarbonate) for 30 min at 56°C and then treated with alkylation solution (55 mM 2-iodoacetamide, 50 mM ammonium bicarbonate) for 30 min under dark condition. The gels were washed by 50 mM ammonium bicarbonate and 100% acetonitrile and dried in a vacuum concentrator. The dried gel pieces were treated with 2 μl of 0.5 μg/μl trypsin (sequence grade; Promega, Madison, WI, USA) and incubated at 37°C for 16 h. The digested peptides in the gel pieces were recovered twice with 20 μl of 5% (v/v) formic acid / 50% (v/v) acetonitrile. Finally, combined extracts were dried in a vacuum concentrator. LC-MS/MS analyses were performed by using an LTQ-Orbitrap XL-HTC-PAL-Paradigm MS4 system. (Thermo Fisher Scientific, Bremen, Germany). MS/MS spectra were analyzed using the in-house MASCOT server (Perkins et al., 1999) (http://www.matrixscience.com/), and the results were annotated with proteins registered in TAIR8.

RT-PCR analysis

Total RNA was isolated from flowers, flower stalks, leaves, and roots of 4-week-old plants using a Sepasol(R)-RNA I Super G kit (Nacalai Tesque, Kyoto, Japan). After DNase treatment, reverse transcription was performed using the Transcriptor First Strand cDNA Synthesis kit (Roche) with an oligo$(dT)_{18}$ primer. The primers used were as follows: 5′-AGAATGGACGGAAACGTGGGC-3′ and 5′-CGTAGCTTCATGCTGCACCACA-3′ for *LINC1*; 5′-CCGGAGGAGGATGAGGAATATACA-3′ and 5′-CTTGGTCTACAGTCTTCTTCCGTC-3′ for *LINC2*; 5′-AACTCCAAGGAAGCGGCAACG-3′ and 5′-TTTCTGTTTCAACCGTAACAATCTCC-3′ for *LINC3*; 5′-TAACCCCTTCATCTGCCACTCC-3′ and 5′-GATATGACACTCTGGGTATCAGCTTC-3′ for *LINC4*; and 5′-CGTACAACCGGTATTGTGCTGG-3′ and 5′-GTGATTTCTTTGCTCATACGGTC-3′ for *ACTIN2*. All genes were amplified in 30 PCR cycles. PCR products were visualized by ethidium bromide staining.

Construction of GFP and YFP fusion proteins

Each *LINC* fragment was amplified from the genome DNA by PCR using primers 5′-aaggcgcgccATGTCCACGCCGTTGAAGGT-3′ and 5′-ttaggcctCGTCGTCAAGAAAGTCCAAAGCT-3′ for *LINC1*; 5′-ctggtacctgATGACGCCGAGAAGCGAGAC-3′ and 5′-catgcggccgcagTGTAGTGAGAAAAGTCCAAAGCTTCT-3′ for *LINC2*; 5′-aaggcgcgccATGTTCACTCCGCAAAGGAATCGT-3′ and 5′-tttcccgggTGTTGTGAAAAAGACCCAAATCTT-3′ for *LINC3*; and 5′-aaggcgcgccATGGCAACTTCTTCTCGTTCGGA-3′ and 5′-tttcccgggCAGAAATAGCCAAAGGGTATTATTCATCT-3′ for *LINC4*. *LINC1*, *LINC3*, and *LINC4* were cloned into the pSY1 binary vector, which carries a pGPTV-Bar backbone, a *CaMV 35S* promoter derived from pBI101, and *eGFP* (Tsien, 1998). *LINC2* was cloned into pDONR201 (Life Technologies, Carlsbad, California, USA) by BP reaction. Cloned *LINC2* DNA was transferred from the entry clone to the pGWB441 destination vector to generate the *eYFP*-tagged constructs (Nakagawa et al., 2007) by the LR reaction. For own promoter analysis, each LINC fragment was amplified from the genome DNA by PCR using primers 5′-aaggcgcgccATGTCCACGCCGTTGAAGGT-3′ and 5′-ttaggcctCGTCGTCAAGAAAGTCCAAAGCT-3′ for *pLINC1*::*gLINC1*; 5′-ctggtacctgATGACGCCGAGAAGCGAGAC-3′ and 5′-catgcggccgcagTGTAGTGAGAAAAGTCCAAAGCTTCT-3′ for *pLINC2*::*gLINC2*; 5′-aaggcgcgccATGTTCACTCCGCAAAGGAATCGT-3′ and 5′-tttcccgggTGTTGTGAAAAAGACCCAAATCTT-3′ for *pLINC3*::*gLINC3*; and 5′-aaggcgcgccATGGCAACTTCTTCTCGTTCGGA-3′ and 5′-tttcccgggCAGAAATAGCCAAAGGGTATTATTCATCT-3′ for *pLINC4*::*gLINC4*. *LINC1*, *LINC2*, and *LINC4* were cloned into the pENTER1A entry vector Cloned *LINC* DNA was transferred from the

entry clone to the pGWB440 destination vector to generate the *eYFP*-tagged constructs (Nakagawa et al., 2007) by the LR reaction. *LINC3* was cloned into pMM1 binary vector, which carries a pTH35 backbone and *sGFP*.

Wild-type *A. thaliana* plants were transformed by infection with *Agrobacterium tumefaciens*. Transformed plants were inspected by confocal laser scanning microscopy (Zeiss LSM710; Carl Zeiss, Jena, Germany). In complementation analysis, above-described constructs of LINC1-GFP and LINC4-GFP were transformed in *linc1* and *linc4* disruptants, respectively. Transformed plants were inspected by the DeltaVision microscope with the Olympus IX70 stand (Personal DV; Applied Precision).

GUS staining

GUS staining was carried out according to the method described by Jefferson et al. (1987) with some modifications. Samples were pre-fixed by 90% acetone on ice for 15 min. After washed with reaction buffer (50 mM phosphate (pH7.2), 2 mM potassium ferricyanide, 2 mM potassium ferrocyanide, 0.1% NP-40) samples were incubated in 0.5 mM X-Gluc in reaction buffer at 37 C for over night. Samples were post-fixed by 1% glutaraldehyde in reaction buffer at 37 C for 2 h and then they were dehydrated by ethanol series (30, 50, 70, 80, 90, 100%) each for 10 min. They were observed by Olympus BX50 microscope (Olympus, Tokyo, Japan).

Confocal laser scanning microscopy

Fluorescence confocal images of LINC-GFP and -YFP were obtained using a confocal laser scanning microscope (Carl Zeiss) equipped with 458, 488, and 514 nm Ar/Kr laser lines, a 561 nm DPSS laser line, and a 633 nm He/Ne laser line and ×63 1.2-NA oil immersion objective (C-Apochromat, 441777-9970-000; Carl Zeiss), or ×40 0.95-NA dry objective (Plan-Apochromat,

440654-9902-000; Carl Zeiss). Image analysis was performed using LSM image examiner software (Carl Zeiss).. Image analysis was performed using LSM image examiner software (Carl Zeiss) and Adobe Photoshop 6.0 (Adobe Systems).

Observation of mitotic cells in root tips

Sample roots were fixed in 4% (w/v) formaldehyde, freshly prepared from paraformaldehyde, in the PIPES buffer for 1 h. The fixed roots were treated with 0.5% (w/v) Cellulase Onozuka RS and 0.05% (w/v) Pectolyase Y-23 in the PIPES buffer for 45 sec at 37°C. The roots were stained with the Hoechst solution for 10 min. Samples were observed using the DeltaVision microscope with the Olympus IX70 stand (Personal DV; Applied Precision). The images were deconvolved using the constrained iterative algorithm (Swedlow et al., 1997) implemented in SoftWoRx software (Applied Precision).

Flow cytometry

Ploidy levels of leaf cell nuclei from 4-week-old plants were determined by flow cytometry as described in the study by Sugimoto-Shirasu et al. (2002). The ploidy level was determined by flow cytometry using a Ploidy Analyser PA-11 (Partec GmbH), with UV excitation at 366 nm from a mercury arc lamp. Leaves, hypocotyls, or flowers were chopped with a razor blade in Cystain extraction buffer (Partec GmbH), filtered through a 30 μm CellTrics filter (Partec GmbH) into a sample tube, and stained with Cystain fluorescent buffer (Partec GmbH). At least 7000 nuclei were used for each ploidy measurement.

Fluorescence *in situ* hybridization

Fluorescence *in situ* hybridization (FISH) analysis of interphase chromosomes was intrinsically same as previously described (Murata et al., 1997). For FISH using 180bp probes

recognizing centromere, the isolated nuclei from flower buds of 5-weeks-plant were prepared. The flower buds were fixed by Carnoy's solution (acetic acid : ethanol = 3 : 1) for 2 h at r.t.. The buds were treated with cellulase solution (2% Cellulase Onozuka RS, 0.5% Pectolyase in citrate buffer pH4.5) for 2 h at 37°C and then crushed by vigorously pipetting. After filtration by 100 μm mesh, the samples were pasted on slide glass. The 180bp probes were labeled with digoxigenin (DIG)-11-dUTP by DIG nick translation kit (Roche) and DIG was detected by rhodamine conjugated anti-DIG antibodies (Roche). DNA was stained by 1 μg/ml DAPI. The FISH samples were mounted with Prolong gold (Life Technologies), sealed by nail polish, and inspected by the DeltaVision microscope with the Olympus IX70 stand (Personal DV; Applied Precision).

Microarray

As one microarray sample, 8 individual 1-week-old seedlings of wild-type plant or *linc1/linc4* disruptant were sampled from GM plate. The seedlings were homogenized in liquid nitrogen and those total RNA were extracted by RNeasy plant kit with DNase treatment (Qiagen, Hilden, Germany). One wild-type RNA sample and three *linc1/linc4* disruptant RNA samples were checked their quality using a 2100 Bioanalyzer (Agilent Technologies, Palo Alto, CA, USA), were Cy-3 labeled using by Agilent Low Input Quick Amp Labeling kit 1-color (Agilent Technologies). Microarray analysis was performed following the manufacturer's instructions (Agilent Technologies) and as previously described by Yamada et al. (2007). It was used an Agilent 4×44k Gene Expression Array: Arabidopsis thaliana Ver.4 and Agilent microarray scanner (Agilent Technologies)

Analysis of light-dependent nuclear positioning

Light-dependent nuclear positioning was examined as described in the study by Iwabuchi et al. (2010). Leaves were detached from the plants at the petioles, floated on distilled water in a petri

dish, and then kept in darkness for 16 h. The dark-adapted leaves were irradiated with blue light (470 nm) using a light-emitting diode light source system (MIL-C1000T for the light source controller, MIL-U200 for the light source frame, and MIL-B18 for the light-emitting diode; SMS). Light intensity was measured with a quantum sensor and data logger (LI-1400; LI-COR). After dark adaptation or blue light irradiation, sample leaves were fixed and stained by the above-described method. Because nuclei of the *linc* disruptants were spherical, the nucleus getting any contact with the anticlinal walls was defined to be in the light position.

Results

Chapter 1: Identification and phylogenic analysis of *LINC*s

LINC1 and LINC4 in the nuclear lamina fraction may be involved in the maintenance of nuclear morphology

To know whether cytoskeletons play any role in the maintenance of plant nuclear morphology, I semi-quantitatively measured the circularity index and area of the nucleus in leaf epidermal cells of *Arabidopsis thaliana* after treatment with latrunculin B and/or propyzamide (Fig. 1A, B), inhibitors of polymerization of actin filaments and microtubules, respectively. No statistically significant difference was detected in both parameters from the control nuclei in any treatment. Furthermore, nuclei isolated from *A. thaliana* leaf protoplasts retained their spindle shape even after treatment with 1% (v/v) Triton X-100 (Fig. 2A); the shape was the same as that in the leaves (Fig. 2B). The morphology of demembranated nuclei was also maintained after treatment with latrunculin B and/or propyzamide (Fig. 3A–D). Additionally, demembranated nuclei were treated with 2,3-butanedione monoxime (BDM) which is an inhibitor of myosin ATPase activity. BDM also did not affect the morphology of the demembranated nuclei (Fig. 3E). Consequently, I assumed that nuclear morphology is maintained by intranuclear factors such as nuclear lamina components but not by extranuclear factors such as cytoskeletons.

I prepared a crude nuclear lamina fraction from the demembranated nuclei by treatment with DNase and RNase. Mesh-like structures composed of fibrous materials typical of the nuclear lamina were clearly present in electron micrographs of the crude nuclear lamina fraction (Fig. 4A). A total of 660 proteins were identified as putative nuclear lamina proteins by LC-MS/MS of the fraction (Fig. 4B, C and Table 1). Because animal lamins are equipped with DNA-binding activity (Dechat et al., 2008),

I selected 63 of the 660 proteins harboring putative DNA-binding motifs or with unknown functions (Table 2). Two lines exhibiting spherical nuclear shapes in leaf trichome cells (Fig. 5A–C) were screened from T-DNA insertion lines for these 63 genes. One line was a *linc1* disruptant (Fig. 5B) and the other was a *linc4* disruptant (Fig. 5C).

Most of vascular plants have LINC genes

A. thaliana harbors four *LINC* genes (Dittmer et al., 2007; Meier, 2007). LINC1 contains 1132 amino acids with a molecular weight of 129 kDa and a PI of 4.96, LINC2 contains 1128 amino acids with a molecular weight of 130 kDa and a PI of 4.79, LINC3 contains 1085 amino acids with a molecular weight of 127 kDa and a PI of 4.99, and LINC4 contains 1042 amino acids with a molecular weight of 121 kDa and a PI of 5.01. All LINCs have multiple coiled-coil domains on the N terminal and a random domain on C terminal. All LINCs and NMCPs sequences were used for BLAST searches including *Physcomitrella patens*, *Zea mays, Oryza sativa*, *Vitis vinifera*, *Daucus carota* L., and *Apium graveolens*, and then the phylogenetic tree was written based on their conserved N terminal sequences (Fig. 6). All LINC homologues except those of *Physcomitrella patens* could be roughly divided into two groups, namely, LINC1, LINC2, LINC3, and NMCP1 belong to the NMCP1 type ,while LINC4 and NMCP2 belong to the NMCP2 type. Monocots such as *Zea mays* and *Oryza sativa* harbor one each homologue of the two types while dicots such as *Vitis vinifera*, *Daucus carota* L., *Apium graveolens,* and *A. thaliana* harbor more than two homologues of the NMCP1 type other than one NMCP2 type. *Physcomitrella patens* harbors a special type of LINC which dose not seem to belong to any of the two types.

.

Chapter 2: Expression and localization analyses of LINCs

Expression levels of LINC1-LINC3 are high in immature tissues and became lower with tissue maturation.

By RT-PCR, all *LINC* genes appeared to be expressed in the wild-type whole plant body (Fig. 7). I further investigated detailed expression patterns of LINCs fused with β-glucuronidase (GUS) and expressed under the control of native promoter in wild-type plants. The genomic fragments of *LINCs* included the approximately 2-kbp upstream promoter sequences from the translation initiation site and the entire coding sequences (*pLINC*::LINC). In 2 days after germination (DAG), signals of *pLINC1*::gLINC1-GUS and *pLINC2*::gLINC2-GUS were detected in the whole plant body but few signal of *pLINC3*::gLINC3-GUS could be detected (Fig. 8). In cotyledon of 5 DAG plants, strongly signals of *pLINC1*::gLINC1-GUS, *pLINC2*::gLINC2-GUS, and *pLINC3*::gLINC3-GUS were detected (Fig. 9A-C). In cotyledon of 8 DAG plants, signals of *pLINC1*::gLINC1-GUS were maintained, whereas those of *pLINC2*::gLINC2-GUS and *pLINC3*::gLINC3-GUS became lower than in cotyledon of 5DAG plants (Fig. 9D-F). As LINC1-LINC3 signals were very high in the first true leaves of 8 DAG plant, reduction of LINC2 and LINC3 signals occurred only in cotyledon (Fig. 9D'-F'). In the first true leaves of 14 DAG plants, LINC1-LINC3 signals were almost disappeared (Fig. 9G-I). To investigate LINC1-LINC3 expression patterns in roots, *pLINC1*::gLINC1-YFP, *pLINC2*::gLINC2-YFP, and *pLINC3*::gLINC3-GFP were transformed in each single disruptant. LINC1-LINC3 signals were detected strongly at meristematic root tip cells and weakly in differentiated cells (Fig. 10). These results suggested that LINC1-LINC3 were mainly expressed in immature tissues and their expression levels became lower with tissue maturation.

Up until now, I could not detect any signals of *pLINC4*::gLINC4-GUS in wild-type plants and *pLINC4*::gLINC4-YFP in wild-type plants and *linc4* disruptants. I produced

3-kbp-*pLINC4*::gLINC4-YFP and transformed *linc4* disruptants with it; however, the construct could not recover the nuclear morphology of *linc4* disruptants, which suggested that even 3-kbp-*pLINC4* is not enough to express LINC4 although 3-kbp-*pLINC4* sequence begins just after start codon of previous gene sequence.

Individual LINCs exhibit different localization patterns in interphase and mitotic cells

I investigated the intracellular localization of LINC-GFP or -YFP expressed under the control of the cauliflower mosaic virus (CaMV) 35S promoter in the wild-type plants. I confirmed that the abnormal nuclear morphology of *linc1* and *linc4* disruptants was recovered by introducing *LINC1-GFP* and *LINC4-GFP*, respectively, into the disruptants (Fig. 11). As reported previously (Dittmer et al. 2007), LINC1 was mainly localized to the nuclear periphery (Fig. 12A, B) and LINC2 was localized in the nucleoplasm of both leaf and root epidermal cells (Fig. 12C, D). LINC3 was also localized in the nucleoplasm of both epidermal cell types (Fig. 12E, F). Punctate or bundle-like LINC3 structures were detected occasionally (Fig. 12F). LINC3 clearly exhibited a bundle-shape localization pattern along the long axis of the nucleus in trichome cells (Fig. 12G). LINC4 was localized frequently to the nuclear periphery (Fig. 12H, I) as punctate structures of different sizes in both epidermal cell types. Furthermore, the nucleus in *LINC4-GFP*-overexpressing plants was considerably larger than that in the wild-type plants (Fig 12J). The longer axis of leaf epidermal nuclei of the wild-type plants was approximately 30 μm at the longest but that in the *LINC4-GFP*-overexpressing plants reached up to 90 μm. I also investigated the localization pattern of *pLINC*::gLINC-GFP or -YFP introduced into the *linc* disruptants. *pLINC1*::gLINC1-YFP and *pLINC3*::gLINC3-GFP were exclusively localized at nuclear periphery in meristematic cells having spherical nuclei and also in differentiated cells having spindle-shaped nuclei in roots (Fig 13A, C, D, F). *pLINC1*::gLINC1-YFP could recover the nuclear morphology of *linc1* disruptants (Fig 13A). *pLINC2*::gLINC2-YFP was mainly localized at nuclear

periphery but partially in nucleoplasm in meristematic and differentiated cells in roots. Intracellular localization patterns of LINC1-LINC3 were unaffected regardless of the morphological difference in nuclei (Fig 13B, E).

Finally, I investigated the intracellular localization of LINC-GFP or -YFP expressed under the control of CaMV35S promoter in the fixed root apical meristem (Fig. 14). LINC1, LINC3, and LINC4 in interphase cells were mainly localized to the nuclear periphery, whereas LINC2 was in the nucleoplasm. A part of LINC3 was localized in the nucleoplasm, and a part of LINC4 appeared to form punctate structures at the nuclear periphery. LINC1 seemed to be localized on the condensing chromatin during prometaphase to anaphase, whereas other LINCs were localized diffusely in the cytoplasm. LINC1 appeared to be transferred from the decondensing chromatin to the reassembling nuclear envelope during early telophase. A small population of LINC2 was transferred from the cytoplasm to the chromatin surface. LINC3 was also transferred from the cytoplasm to the chromatin surface, as if preferentially assembling to the distal surface of the chromatin (Fig. 14 arrows). LINC4 was assembled into punctate structures in the cytoplasm (Fig. 14 arrowheads) and then to the chromatin surface. All LINCs were localized again to the nuclear periphery during late telophase, and a part of LINC4 was still localized on the punctate structures. These results suggest that individual LINCs exhibit different redistribution patterns during different mitotic phases.

Chapter3: Roles of LINCs for nuclear morphology, movement, ploidy level, chromatin structure, and gene expression

LINC1 and LINC4 play predominant roles in the maintenance of nuclear morphology in leaf and root epidermal cells

linc1–linc4 single disruptants and *linc1/linc4* and *linc2/linc3* double disruptants were prepared to determine which LINC family isoforms were involved in the maintenance of nuclear morphology. Disruption of these distinctive genes was confirmed by RT-PCR using gene-specific primers (Fig. 15). No detectable difference in the whole-plant morphology was obvious between any of the *linc* disruptants and wild-type plants at least under the present growth conditions (Fig. 16).

I semi-quantitatively measured the circularity index and area of the nucleus in the leaf and root epidermal cells of *linc* disruptants. In leaf epidermal cells, the circularity index of the nucleus in all *linc* disruptants except *linc3* was significantly higher than that in the wild-type plants (Fig. 17A). The extent of the effects of *LINC1*, *LINC4*, and *LINC1/LINC4* disruption was significantly higher than that of the effects of *LINC2* and *LINC2/LINC3* disruption. The nuclear area in the *linc1*, *linc4*, and *linc1/linc4* disruptants was significantly smaller than that in the wild-type plants, while the nuclear area in the *linc2*, *linc3*, and *linc2/linc3* disruptants was not significantly different from that in the wild-type plants (Fig. 17B). Neither the nuclear circularity index nor the nuclear area in the *linc1*, *linc4*, and *linc1/linc4* disruptants were significantly different from each other, suggesting that both LINC1 and LINC4 are factors indispensable for maintaining nuclear morphology in leaf epidermal cells. More or less similar results were obtained in root epidermal cells, except that *LINC3* disruption resulted in a small but significant effect on the nuclear circularity index (Fig. 17C, D). In summary, although all *LINC* genes were expressed in the whole plant body, LINC1 and LINC4 functioned predominantly and LINC2 subordinately in the regulation of nuclear morphology in leaf and root

epidermal cells. LINC3 functioned in roots but not or redundantly functioned with other LINCs in leaves.

Leaf epidermal cells of all *linc* disruptants exhibit normal light-dependent nuclear positioning

I investigated the effects of *LINC* disruption on light-dependent nuclear positioning to determine whether nuclear morphology affects nuclear movement. Nuclei of the leaf cells of *A. thaliana* relocate from the center of the bottom of cells to the anticlinal walls in response to strong blue light (Iwabuchi et al., 2007). Only 40% nuclei of the leaf epidermal cells of the wild-type plants were located along the anticlinal walls under the dark condition, whereas 80% nuclei were along the anticlinal walls after blue light illumination at 100 μmol m^{-2} s^{-1} for 5 h (Fig. 18). All *linc* disruptants exhibited almost normal light-dependent nuclear positioning, indicating that LINCs are not involved in the regulation of nuclear movement, and that nuclear morphology may not affect nuclear movement in leaf epidermal cells.

Leaf cells of all *linc* disruptants exhibit a normal ploidy level

Because nuclear morphology in leaf epidermal cells was altered in most of the *linc* disruptants, I analyzed DNA content in nuclei isolated from rosette leaves by flow cytometry. As reported previously, nuclei from the wild-type leaves had widely distributed DNA content ranging from 2C to 32C (Melaragno et al., 1993; Sugimoto-Shirasu and Roberts, 2003; Ishida et al., 2008), with the highest population of nuclei containing 8C in 4-week-old plants (Fig. 19). Nuclei of all *linc* disruptants exhibited almost identical patterns of DNA content compared with the nuclei of the wild-type plants. Thus, LINCs may not be involved in the determination of the ploidy level, at least in leaf cells.

linc1/linc4 disruptant exhibits abnormal chromatin distribution

The chromatin architecture was analyzed by fluorescence *in situ* hybridization (FISH) in wild-type plants and *linc1/linc4* disruptants. A digoxigenin-labeled 180-bp DNA probe and a 45S-rDNA probe, whose sequences were complementary with the sequence of centromere contained in all chromosomes and that of 45S ribosomal DNA contained in chromosome II and IV, respectively (Fig. 21G), were detected by rhodamine-conjugated anti-digoxigenin antibodies. Sample nuclei were isolated form flower buds of 5-week-old plants. The number of 180-bp DNA signal foci per one nucleus in wild-type plants was larger than that in *linc1/linc4* disruptants, whereas the size of foci in wild-type plants was smaller than that in *linc1/linc4* disruptants (Fig. 20). The population of nucleus having 10 foci was the largest in wild-type plants because almost nuclei from flower buds have 2C DNA, which corresponds to 10 chromosomes and 10 centromeres (one chromosome contains one centromere). However, in *linc1/linc4* disruptants, the population of nucleus having 10 foci was very small and 4-6 foci became larger. The average fluorescence intensity of 180-bp DNA signals per one nucleus in *linc1/linc4* disruptants was not lower than that in wild-type plants (Fig. 20H), suggesting that reduction in the number of foci did not reflect reduction in the amount of centromere in *linc1/linc4* disruptants. In the case of 45S-rDNA probes, the number of foci was 2-4 in wild-type plants; however, there were nuclei having only 1 focus in *linc1/linc4* disruptants (Fig. 21A-F). The results obtained by flow cytometry and FISH suggested that LINC1 and LINC4 regulate chromatin architecture without alteration of ploidy level.

Discussion

LINC family proteins are involved in the regulation of nuclear morphology

In this study, I showed that all LINCs were involved in the regulation of nuclear morphology, although the extent of the effects of disruption of individual *LINC* genes was different. Of note, other than the known factor LINC1 (Dittmer et al., 2007), LINC4 also plays predominant non-redundant roles with LINC1 in leaf and root epidermal cells (Fig. 17). According to the previous report, native promoter driven LINC1-GFP, introduced into the *linc1/linc2* disruptants, was expressed only in the root proliferating meristematic tissues but not in differentiated root tissues, such as mature root hairs and epidermal cells (Dittmer and Richards, 2008). In my data, LINC1-LINC3 expression levels in immature tissues are higher than in matured and differentiated tissues (Figs. 8-10). It is intriguing that the abnormal nuclear shape of the *linc1* disruptants is most marked in differentiated tissues, in which the LINC1 promoter activity is not high. On the basis of phylogenetic analysis (Fig. 6, Kimura et al., 2010; Ciska et al., 2013), LINCs have been classified into the NMCP1 type containing LINC1–3 and the NMCP2 type containing LINC4. NMCP1- and NMCP2-type proteins may play different and essential roles co-operatively for the determination and/or maintenance of nuclear morphology. These possibilities should be examined.

Plants utilize multiple isoforms of key proteins, expressed in developmental stage-, tissue-, or cell type-specific manners, to fulfill growth, development, and adaptation. For example, the eight *A. thaliana* PIN-FORMED proteins (PINs) are auxin efflux carriers, and each PIN isoform functions in a specific tissue or cell type to induce tissue- and cell type-specific auxin flow (Křeček et al., 2009). A similar aspect has been reported in the primary transporter plasma membrane H^+-ATPase proteins (Palmgren, 2001; Arango et al., 2003). Nuclei of the root epidermal cells of the *linc3* disruptant were more spherical than those of the wild-type plants (Fig. 17C), although nuclei of the leaf epidermal

cells appeared to maintain a normal shape (Fig. 17A). It is suggested that different combinations of LINCs and interactions with their partners contribute to the diversity in plant nuclear morphology.

Regulation of nuclear morphology was accomplished through two steps

LINC1-LINC3 are highly expressed in immature tissues (Figs. 8-10) having mainly spherical and elongating nuclei and their expression levels become lower in mature tissues (Figs. 9, 10) having mainly elongated and spindle shaped nuclei. Spindle shaped nuclei maintained their morphology even after treatment with cytoskeletal inhibitors *in vivo* and *in vitro* (Figs. 1, 3) On the other hand, Tamura et al. (2013) demonstrated that myosin XI-I is localized at nuclear periphery and involved in the regulation of nuclear morphology. These facts suggest that regulation of nuclear morphology is accomplished through at least two steps; one is a strain step and the other is a maintenance step. In the strain step, actin and myosin XI-I generate a force that is transferred into the nucleus through the SUN-KASH complex. The force is received by LINC1-LINC3 to deform the nuclear envelopes. In the maintenance step, the force generated by cytoskeletons is no longer need but intranuclear factors keep the spindle shaped nuclear morphology. Although I have not yet revealed the expression patterns of LINC4, since the effects of disruption are independent of other LINCs, LINC4 could be one of the possible candidates of the intranuclear factors. Defects of any of those factors make the nucleus the most geometrically stable shape a sphere.

LINCs exhibit distinctive localization patterns in the nucleus of interphase cells

LINC1 was localized to the nuclear periphery and LINC2 was localized in the nucleoplasm of both leaf and root epidermal cells (Figs. 12A-D, 13A, B, D, E), confirming previous results (Dittmer et al., 2007). LINC3 was localized to the nuclear periphery and nucleoplasm in punctate and bundle-shaped structures (Figs. 12E-G and 13C, F). LINC4 was localized to the nuclear periphery in

punctate structures (Fig. 12H-J). Although these characteristic structures might be the results of overexpression, the appearance of bundle-shaped structures suggests that LINC3 may have the ability to polymerize *in vivo*. In leaf epidermal cells, *LINC4*-overexpressing plants exhibited considerably longer nuclei than the wild-type plants (Fig. 12J). This was similar to the case of the leaf cells of *NUCLEOPORIN136* (*Nup136)*-overexpressing plants, which also have longer nuclei (Tamura and Hara-Nishimura, 2011). Plant Nup136 is a component of the nuclear pore complex (Lu et al., 2010; Tamura et al., 2010) and thought to be a functional homolog of animal Nup153, which interacts with lamin A and B in *Xenopus* (Smythe et al., 2000; Al-Haboubi et al., 2011). Nuclear morphology and nuclear lamina architecture in *Nup153 K.D.* HeLa cells are impaired (Zhou and Panté, 2010). These results suggest that LINC4 may interact with Nup136 to maintain the spindle shape of plant nuclei.

LINCs exhibit different redistribution patterns in mitotic cells

Inner nuclear envelope proteins such as LBR and Lap-Emerin-Man (LEM) domain proteins are localized to the mitotic endoplasmic reticulum (ER) during mitosis in animal cells (Ellenberg et al., 1997; Yang et al., 1997; Güttinger et al., 2009; Hetzer, 2010), whereas lamins, which interact with LBR and LEM domain proteins during interphase, are dispersed in the cytoplasm from metaphase to anaphase (Yang et al., 1997; Burke and Ellenberg, 2002). In plant cells, the ectopically expressed N-terminal region of human LBR (Irons et al., 2003; Evans et al., 2011) and full-length proteins of *A. thaliana* SUN1 and SUN2 (Oda and Fukuda, 2011; Graumann and Evans, 2011) are also localized to the mitotic ER from metaphase to anaphase. These two initially relocate from the mitotic ER to the cell plate and the distal surface of chromosomes during early telophase and then further to the proximal surface of chromosomes during late telophase. The localization pattern of another group of nuclear peripheral proteins lacking transmembrane domains, NMCP1 and NMCP2, which contain sequences homologous to LINCs, has been reported in embryogenic *D. carota* L. cells and

suspension-cultured *Apium graveolens* cells (Masuda et al., 1999; Kimura et al., 2010). Both proteins reside at the nuclear periphery during interphase. NMCP1 relocates to the spindle during metaphase and then accumulates at the surface of chromosomes during anaphase. In contrast, NMCP2 is dispersed throughout the cytoplasm from metaphase to the end of anaphase and then accumulates at the surface of chromosomes in telophase, but later than NMCP1 accumulation.

In my study, the localization pattern of LINCs in mitotic cells was observed for the first time, although they were expressed under the control of the CaMV 35S promoter. LINC1 appeared to be associated with chromosomes throughout mitosis (Fig. 14), which was different from any of the inner nuclear envelope proteins and NMCPs that are localized to the mitotic ER, cell plate, spindle, or cytoplasm, but not to chromosomes (Masuda et al., 1999; Irons et al., 2003; Kimura et al., 2010; Evans et al., 2011; Oda and Fukuda, 2011; Graumann and Evans, 2011). Only histone H1, which is localized to the nuclear periphery and nucleoplasm during S/G2 phase, is associated with chromosomes during mitosis in tobacco BY-2 cells (Hotta et al., 2007; Nakayama et al., 2008), suggesting that LINC1 may associate with DNA. From prometaphase to anaphase, other LINCs exhibited almost identical localization patterns (Fig. 14), in which they were dispersed in the cytoplasm similar to animal lamins and NMCP2 rather than plant inner nuclear envelope proteins (Yang et al., 1997; Masuda et al., 1999; Burke and Ellenberg, 2002; Irons et al., 2003; Kimura et al., 2010; Evans et al., 2011; Oda and Fukuda, 2011; Graumann and Evans, 2011). A part of LINC2 was assembled around chromosomes during early telophase. LINC3 was first assembled at the distal surface of chromosomes as an inner nuclear envelope protein, which is the ER-specific localization patterns revealed in SUN1, SUN2 (Oda and Fukuda, 2011; Graumann and Evans, 2011) and ectopically expressed truncated LBR (Irons et al., 2003; Evans et al., 2011) were never observed. LINC4 first accumulated in the cytoplasmic punctate structures, which have not been reported in the plant inner nuclear envelope or nuclear peripheral proteins, and then was assembled at the surface of chromosomes during late telophase. In animal cells,

lamins, some of the nuclear pore complexes, and some of the inner nuclear envelope proteins are phosphorylated when they relocate from the nuclear periphery during mitosis (Dessev and Goldman 1988; Dessev et al., 1988, 1989, 1990; Burke and Ellenberg, 2002), suggesting that redistribution of plant LINCs during mitosis is also regulated through phosphorylation and dephosphorylation.

Regulation of DNA content and nuclear morphology is independent

All *linc* disruptants appeared to maintain the normal ploidy level (Fig. 19), although the nuclear area in the leaf epidermal cells of the *linc1* and *linc4* disruptants was significantly smaller than that of the wild-type plants (Fig. 17B). Although the ploidy level was only slightly lower in the *linc1*/2 double disruptants (Dittmer et al., 2007) than in the wild-type plants, nuclear volume decreased dramatically with a concomitant increase in DNA density. Similarly, the DNA density of nuclei of the *linc1* and *linc4* disruptants might also be higher than that in the wild-type plants. From the results obtained in the *linc* disruptants in this study and in the study by Dittmer et al. (2007), I assume that regulatory mechanisms for the ploidy level and nuclear volume are separable, at least in part.

Nuclear morphology does not affect nuclear movement

Extranuclear force is necessary in animal cells for nuclear movement and the maintenance of nuclear morphology. The mouse fibroblast nucleus moves rearward in the cell before the start of migration (Gomes et al., 2005; Luxton et al., 2010). The nuclei of developing neuroepithelial cells move in an apical–basal manner and in-phase with the cell cycle (Baye and Link, 2008). These nuclear migrations depend on the presence of the SUN-KASH complex and cytoskeletons, which transmit the extranuclear force into the nucleus. Nuclear movement and the maintenance of nuclear morphology partly share this machinery in animal cells.

I examined light-dependent nuclear positioning in the *linc* disruptants to determine whether

LINCs play a role in nuclear movement and/or positioning, but they showed a normal response (Fig. 18). Although nuclei in the *sun1-K.D./sun2-K.D.* plants are more spherical than those in the wild-type plants, nuclear movement in the root hair cells of the *sun1-K.D./sun2-K.D.* plants does not differ from that of the wild-type plants (Oda and Fukuda, 2011). However, a resent report showed *myosin xi-i* and *wit1/wit2* mutants exhibited both phenotype spherical nuclear morphology and slow nuclear movements (Tamura et al., 2013). These observations suggest that the mechanism for the maintenance of nuclear morphology in plant cells partially common with that for nuclear movement and/or positioning however that nuclear morphology does not considerably affect nuclear movement and/or positioning.

LINC disruptions do not seem to be serious for plant life

Although LINC disruptions affected nuclear morphology, size, and chromatin architectures, at least LINC single and LINC1/LINC4 and LINC2/LINC3 double disruptions did not affect plant growth and development under the present experimental conditions (Figs. 16, 17, 20, 21). LINC1/LINC2 double disruption induced plant dwarf phenotype but it was neither so serious (Dittmer et al., 2007). The disruption of SUN1 and SUN2 proteins, which are inner nuclear envelop proteins and interact with KASH proteins, induced similar phenotype as LINC disruption. The *sun1*-K.D./*sun2*-K.D. plants exhibited small and spherical nuclear morphology but no significant differences in development or fertility compared with wild-type plants (Oda et al., 2011). Additionally, the disruption of condensin, which is a multimeric protein complex involved in the chromosome condensation during mitosis and meiosis and regulation of chromatin territory during interphase, also induced similar phenotype. Condensin complex is presumably constituted by one of three different SMC4A-C subunits, one of two different SMC2A, B subunits, one of different CAP-H, H2 subunits, one of two different CAP-D2, D3 subunits and CAP-G, G2 subunits. One of the condensin component

mutants (*cap-D3*) exhibited lower number of centromere signals than wild-type plants and small plant body size (Schubert et al., 2013). However, other mutants of condensin component (CAP-G2 and CAP-H2 disruption) exhibited higher DNA double-strand breaks levels and shorter roots than wild-type plants in the presence of a double-strand breaks inducing reagent zeocin or under UV-C (Sakamoto et al., 2011). These studies and my results suggested that defects in nuclear morphology and chromatin architecture may induce more DNA damage under stressed conditions, such as under UV irradiation. LINC homologous genes were only found in land plants (Fig. 6, Ciska et al., 2013), which might suggest that plants had acquired LINC genes in order to protect DNA from UV damage and succeeded in being terrestrial.

Figures

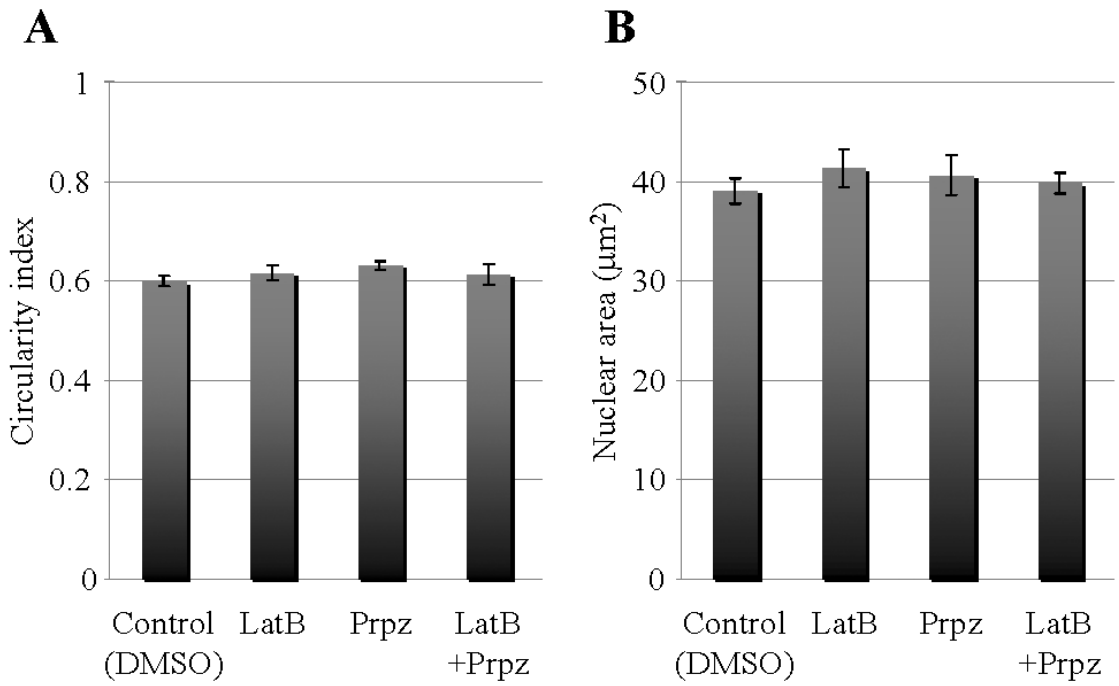

Figure 1

Effects of latrunculin B and propyzamide on the nuclear morphology in *Arabidopsis thaliana*

Leaves were treated for 1 h with 10 μM latrunculin B (LatB) and/or 100 μM propyzamide (Prpz), or with 1% DMSO as control, before fixation. The nuclear circularity index (A) and nuclear area (B) were semi-quantitated from fluorescence images of nuclei stained with Hoechst in the leaf epidermal cells of the wild-type plants. No difference was detected from the control nuclei in any experiments by Student's *t*-test ($p > 0.05$). Four different plants and more than 60 nuclei in each were analyzed for each experiment. The vertical bars on each column indicate the standard error.

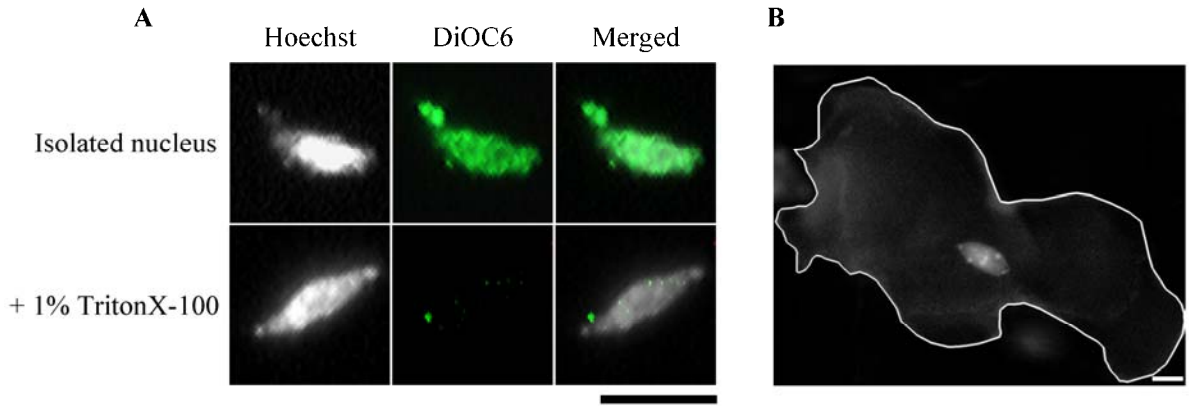

Figure 2

Morphology of nuclei in *A. thaliana* leaves

Fluorescence images of isolated nuclei from leaves stained with Hoechst (left panels) and 3′-dihexyloxacarbocyanine iodide (middle panels) before (upper panels) and after (lower panels) treatment with 1% (v/v) Triton X-100 (A). Merged images are shown in the right panels. Fluorescence image of a leaf epidermal cell stained with Hoechst (B). The white line traces an epidermal cell. Scale bars are 10 µm.

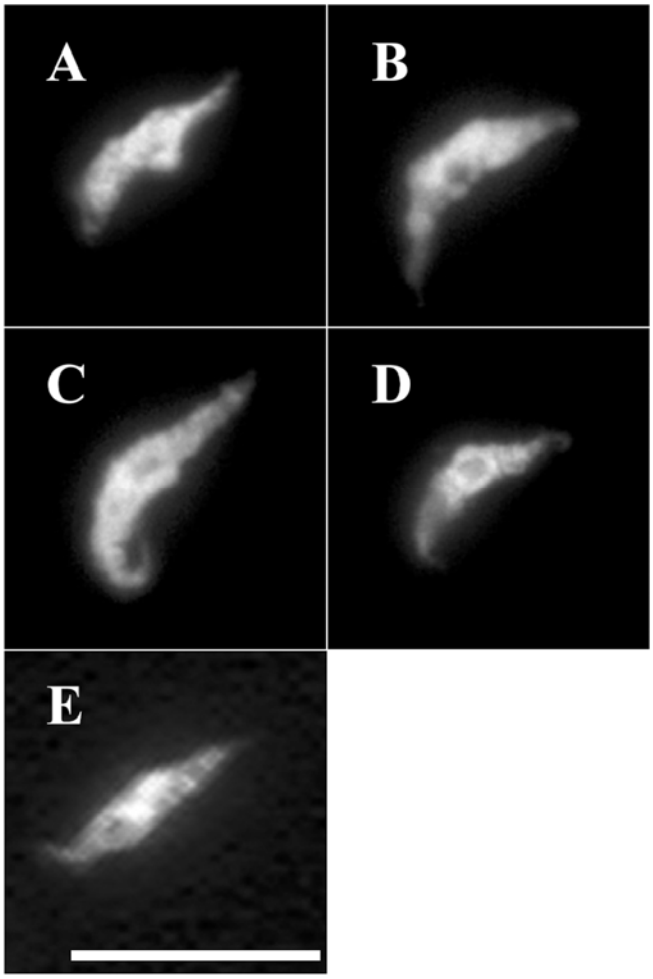

Figure 3

Effects of latrunculin B, propyzamide, and BDM on the demembranated nuclear morphology in *A. thaliana*

Demembranated nuclei isolated from wild-type plant leaves were visualized by staining with Hoechst after 1% DMSO (A), 10 μM LatB (B), 100 μM Prpz (C), 10 μM LatB and 100 μM Prpz (D), or 100 μM BDM (E) treatment. Scale bar is 10 μm

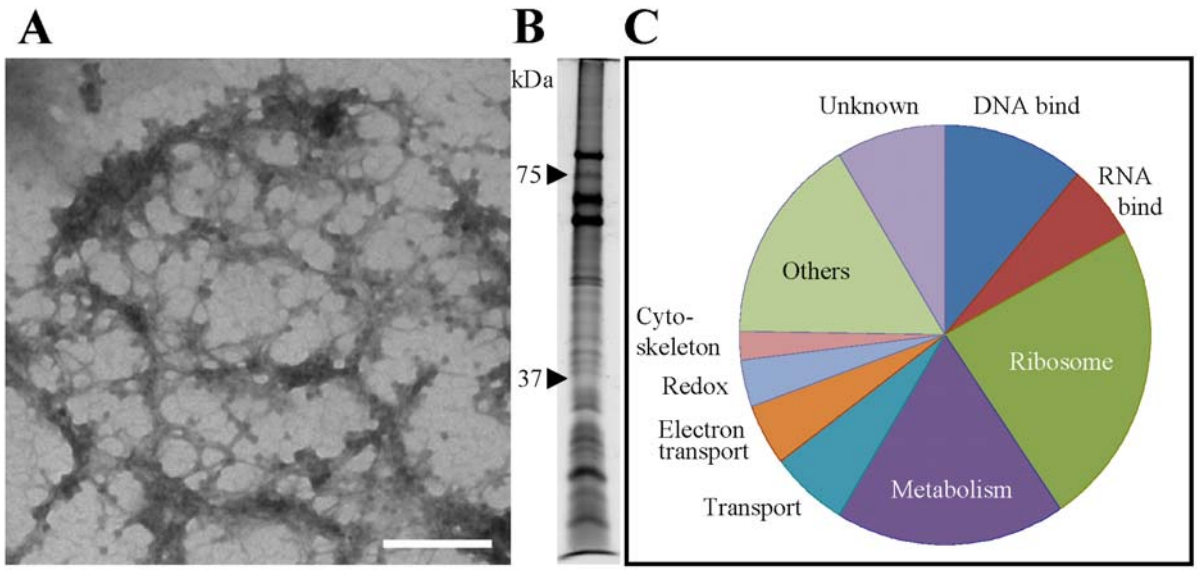

Figure 4

LC-MS/MS analysis in the crude nuclear lamina fraction prepared from *A. thaliana* leaves

An electron micrograph (A) and a sodium dodecyl sulfate-polyacrylamide gel electrophoresis (SDS-PAGE) pattern (B) of the nuclear lamina fraction prepared from the wild-type plants. The molecular masses of standard proteins are indicated on the left in kDa. (C) Proteins contained in the nuclear lamina fraction were analyzed by liquid chromatography-tandem mass spectroscopy (LC-MS/MS) and annotated using the MASCOT and TAIR8 databases according to their deduced functions. The scale bar is 200 nm in (A)

	AGI code	Score	Peptide
1	AT1G01080.1	232	6
2	AT1G01320.1	452	25
3	AT1G01620.1	80	3
4	AT1G02140.1	62	3
5	AT1G03130.1	98	6
6	AT1G03880.1	101	2
7	AT1G04040.1	68	7
8	AT1G04170.1	300	20
9	AT1G04270.1	122	6
10	AT1G04430.1	66	3
11	AT1G04480.1	133	8
12	AT1G04820.1	107	3
13	AT1G04980.1	182	9
14	AT1G05190.1	468	17
15	AT1G06220.1	1563	72
16	AT1G07320.1	420	14
17	AT1G07360.1	80	2
18	AT1G07660.1	620	27
19	AT1G07770.1	195	11
20	AT1G07790.1	1186	64
21	AT1G07920.1	253	19
22	AT1G08450.1	114	6
23	AT1G08640.1	85	1
24	AT1G09080.1	114	8
25	AT1G09200.1	103	17
26	AT1G09340.1	1396	74
27	AT1G09590.1	101	9
28	AT1G09760.1	162	4
29	AT1G09770.1	164	14
30	AT1G10290.1	376	19
31	AT1G10300.1	66	3
32	AT1G10580.1	331	15
33	AT1G10630.1	95	2
34	AT1G10840.1	298	9
35	AT1G12900.1	145	5
36	AT1G13370.1	63	10
37	AT1G14320.1	171	4
38	AT1G14830.1	120	6
39	AT1G14850.1	221	11
40	AT1G15290.1	84	6
41	AT1G15440.1	150	8
42	AT1G15820.1	190	9
43	AT1G15930.1	67	1
44	AT1G16030.1	116	5
45	AT1G16720.1	153	6
46	AT1G16790.1	62	1
47	AT1G18080.1	301	9
48	AT1G18450.1	239	16
49	AT1G18540.1	208	9
50	AT1G18850.1	116	3
51	AT1G19880.1	61	6
52	AT1G20020.1	249	15
53	AT1G20580.1	76	4
54	AT1G20600.1	63	2
55	AT1G20620.1	323	23
56	AT1G20630.1	160	5
57	AT1G20960.1	2413	137
58	AT1G22530.1	86	3
59	AT1G22610.1	114	9
60	AT1G22780.1	205	8
61	AT1G23310.1	73	4
62	AT1G23410.1	167	21
63	AT1G24310.1	80	4
64	AT1G24360.1	766	21
65	AT1G24706.1	407	20
66	AT1G26880.1	101	2
67	AT1G26910.1	136	4
68	AT1G27400.1	174	8
69	AT1G29910.1	220	9
70	AT1G29940.1	71	8
71	AT1G31330.1	316	17
72	AT1G31340.1	144	15
73	AT1G31850.1	84	6
74	AT1G32060.1	79	2
75	AT1G32900.1	8653	392
76	AT1G32990.1	131	6
77	AT1G33120.1	587	19
78	AT1G33410.1	125	13
79	AT1G34430.1	232	9
80	AT1G35680.1	254	9
81	AT1G36240.1	125	5
82	AT1G41880.1	98	5
83	AT1G42430.1	147	13
84	AT1G42970.1	142	9
85	AT1G43170.1	379	26
86	AT1G44575.1	345	13
87	AT1G47128.1	125	4
88	AT1G48350.1	78	7
89	AT1G48610.1	362	19
90	AT1G49240.1	171	7
91	AT1G49670.1	524	24
92	AT1G49750.1	633	29
93	AT1G50920.1	252	12
94	AT1G51060.1	493	17
95	AT1G51570.1	211	11
96	AT1G52230.1	100	2
97	AT1G52360.1	215	14
98	AT1G52400.1	113	5
99	AT1G52740.1	270	12
100	AT1G54270.1	220	10
101	AT1G54690.1	400	19
102	AT1G55490.1	232	12
103	AT1G55670.1	77	4
104	AT1G56070.1	129	12
105	AT1G56110.1	280	18
106	AT1G56190.1	213	9
107	AT1G56410.1	215	12
108	AT1G57660.1	101	10
109	AT1G59610.1	461	24
110	AT1G59760.1	70	8
111	AT1G61520.1	362	9
112	AT1G61730.1	171	6
113	AT1G62020.1	222	15
114	AT1G62330.1	68	2
115	AT1G63680.1	146	10
116	AT1G65260.1	282	11
117	AT1G65350.1	146	9
118	AT1G65440.2	84	5
119	AT1G67090.1	158	12
120	AT1G67230.1	936	60
121	AT1G67430.1	148	9
122	AT1G67680.1	307	21
123	AT1G68830.1	82	2
124	AT1G68910.1	139	5
125	AT1G69200.1	97	9
126	AT1G70070.1	109	8
127	AT1G70580.1	68	2
128	AT1G70770.1	71	8
129	AT1G71040.1	272	16
130	AT1G71695.1	1004	37
131	AT1G72150.1	101	3
132	AT1G72370.1	304	8
133	AT1G72730.1	189	10
134	AT1G73990.1	121	12
135	AT1G74050.1	227	10
136	AT1G74470.1	79	4
137	AT1G74850.1	448	25
138	AT1G74970.1	218	10
139	AT1G75350.1	95	3
140	AT1G75780.1	76	4
141	AT1G76300.1	78	2
142	AT1G77180.1	136	11
143	AT1G77940.1	125	5
144	AT1G78630.1	383	19
145	AT1G78900.1	530	25
146	AT1G79150.1	78	9
147	AT1G79850.1	182	6
148	AT1G79990.1	143	6
149	AT1G80030.1	140	8
150	AT1G80070.1	1753	127
151	AT1G80380.1	72	4
152	AT1G80410.1	383	22
153	AT1G80680.1	130	3
154	AT1G80930.1	152	7
155	AT2G01250.1	448	20
156	AT2G01720.1	77	6
157	AT2G04030.1	97	6
158	AT2G04390.1	110	5
159	AT2G04842.1	102	7
160	AT2G05070.1	139	7
161	AT2G05120.1	142	12
162	AT2G06210.1	267	12
163	AT2G07360.1	215	11
164	AT2G07640.1	83	4
165	AT2G07698.1	169	9
166	AT2G09990.1	172	8
167	AT2G10940.1	134	4
168	AT2G14120.1	82	8
169	AT2G14720.1	75	2
170	AT2G15400.1	73	2
171	AT2G15430.1	117	5
172	AT2G16430.2	343	14
173	AT2G17250.1	69	6
174	AT2G17360.1	275	17
175	AT2G18020.1	229	11
176	AT2G18220.1	60	3
177	AT2G18740.1	159	8
178	AT2G18900.1	74	10
179	AT2G19480.1	174	9
180	AT2G19520.1	108	8
181	AT2G20260.1	101	3
182	AT2G20450.1	132	7
183	AT2G20580.1	120	8
184	AT2G20990.1	286	25
185	AT2G21390.1	272	17
186	AT2G21580.1	238	10
187	AT2G21660.1	110	4
188	AT2G22230.1	405	14
189	AT2G22360.1	71	3
190	AT2G23070.1	88	3
191	AT2G23930.1	63	2
192	AT2G24060.1	122	7
193	AT2G24090.1	71	2
194	AT2G24420.1	115	2
195	AT2G24820.1	368	20
196	AT2G27170.1	640	44
197	AT2G27710.1	78	1
198	AT2G28000.1	86	8
199	AT2G28720.1	1197	64
200	AT2G28900.1	135	4
201	AT2G30620.1	147	8
202	AT2G31610.1	333	13
203	AT2G32920.1	259	13
204	AT2G33150.1	87	5
205	AT2G33450.1	104	5
206	AT2G33800.1	362	15
207	AT2G34420.1	220	8
208	AT2G34430.1	162	7
209	AT2G34480.1	198	11
210	AT2G34970.1	161	11
211	AT2G35960.1	68	2
212	AT2G36130.1	77	4
213	AT2G36160.1	164	9
214	AT2G36390.1	114	10
215	AT2G36620.1	96	2
216	AT2G37170.1	66	3
217	AT2G37190.1	239	5
218	AT2G37270.1	120	5
219	AT2G37470.1	1072	59
220	AT2G37620.1	76	7
221	AT2G38040.1	465	25
222	AT2G38140.1	60	4
223	AT2G38770.1	908	42
224	AT2G38810.1	284	11
225	AT2G39010.1	72	2
226	AT2G39390.1	117	8
227	AT2G39460.1	175	9
228	AT2G39730.1	306	15
229	AT2G39810.1	414	20
230	AT2G39850.1	127	4
231	AT2G39990.1	281	7
232	AT2G40010.1	155	6
233	AT2G40360.1	62	8
234	AT2G40510.1	110	2
235	AT2G40660.1	299	16
236	AT2G41620.1	636	26
237	AT2G42270.1	388	31
238	AT2G42740.1	273	8
239	AT2G43030.1	623	23
240	AT2G43640.1	94	3
241	AT2G43770.1	105	7
242	AT2G44120.1	401	21
243	AT2G44530.1	80	1
244	AT2G45640.1	138	9
245	AT2G45710.1	111	2
246	AT2G45960.1	63	3
247	AT2G46110.1	98	3
248	AT2G47610.1	250	14
249	AT2G47980.1	96	6
250	AT2G47990.1	67	4
251	AT3G01060.1	75	6
252	AT3G01180.1	717	39
253	AT3G01500.1	118	4
254	AT3G01780.1	451	23
255	AT3G02080.1	222	14
256	AT3G02200.2	648	19
257	AT3G02760.1	112	9
258	AT3G03920.1	135	5
259	AT3G03960.1	186	4
260	AT3G04230.1	61	2
261	AT3G04260.1	94	3
262	AT3G04600.1	404	15
263	AT3G04840.1	117	7
264	AT3G04920.1	108	4
265	AT3G05060.1	448	17
266	AT3G05560.1	190	7
267	AT3G05590.1	164	9
268	AT3G05970.1	265	19
269	AT3G06400.1	571	25
270	AT3G06510.1	290	16
271	AT3G06530.1	299	19
272	AT3G06730.1	158	3
273	AT3G06810.1	715	40
274	AT3G06860.1	293	26
275	AT3G07050.1	78	2
276	AT3G07110.1	147	8
277	AT3G07770.1	64	4
278	AT3G08530.1	285	15
279	AT3G08580.1	159	5
280	AT3G08940.2	214	7
281	AT3G09480.1	314	35
282	AT3G09500.1	220	11
283	AT3G09630.1	765	33
284	AT3G09680.1	86	2
285	AT3G09790.1	144	8
286	AT3G10530.1	63	9
287	AT3G10690.1	218	12
288	AT3G10730.1	154	8
289	AT3G10950.1	79	4
290	AT3G11130.1	314	10
291	AT3G11510.1	161	9
292	AT3G11630.1	77	3
293	AT3G11660.1	78	4
294	AT3G11710.1	225	18
295	AT3G11830.1	76	6
296	AT3G11940.1	120	5
297	AT3G11964.1	215	18
298	AT3G12110.1	80	7
299	AT3G12390.1	139	5
300	AT3G12580.1	247	15

	AGI code	Score	Peptide
401	AT3G60830.1	150	6
402	AT3G61050.1	107	9
403	AT3G61470.1	74	1
404	AT3G62600.1	86	5
405	AT3G62870.1	224	13
406	AT3G63130.1	357	19
407	AT3G63140.1	722	39
408	AT3G63160.1	62	2
409	AT3G63490.1	343	19
410	AT4G00270.1	98	4
411	AT4G01310.1	298	11
412	AT4G02520.1	117	3
413	AT4G02840.1	94	2
414	AT4G03430.1	121	10
415	AT4G04640.1	178	6
416	AT4G04940.1	192	10
417	AT4G05420.1	122	6
418	AT4G05530.1	147	3
419	AT4G07410.1	176	8
420	AT4G10320.1	884	40
421	AT4G10340.1	277	7
422	AT4G10750.1	325	12
423	AT4G11010.1	227	16
424	AT4G11380.1	92	7
425	AT4G11420.1	631	39
426	AT4G13170.1	147	8
427	AT4G13940.1	107	6
428	AT4G14960.1	72	4
429	AT4G15000.1	126	8
430	AT4G15900.1	122	6
431	AT4G16143.1	86	3
432	AT4G16150.1	108	5
433	AT4G16155.1	96	8
434	AT4G16680.1	75	3
435	AT4G16720.1	125	4
436	AT4G17560.1	84	9
437	AT4G18100.1	108	11
438	AT4G18360.1	83	4
439	AT4G18465.1	423	21
440	AT4G19120.1	92	6
441	AT4G20130.1	279	14
442	AT4G20360.1	527	16
443	AT4G21150.1	488	18
444	AT4G21710.1	229	14
445	AT4G24190.1	415	19
446	AT4G24280.1	109	12
447	AT4G24820.1	248	10
448	AT4G25210.1	86	3
449	AT4G25340.1	132	10
450	AT4G25630.1	357	15
451	AT4G26110.1	249	18
452	AT4G26270.1	127	5
453	AT4G26630.1	216	13
454	AT4G26840.1	95	3
455	AT4G26910.1	141	8
456	AT4G27090.1	196	11
457	AT4G27230.1	453	16
458	AT4G27740.1	63	3
459	AT4G28080.1	164	17
460	AT4G28200.1	77	9
461	AT4G28520.1	419	15
462	AT4G28750.1	108	4
463	AT4G29010.1	624	46
464	AT4G29220.1	249	9
465	AT4G30330.1	168	7
466	AT4G30690.1	117	7
467	AT4G31480.1	115	11
468	AT4G31700.1	121	5
469	AT4G31880.1	67	3
470	AT4G32910.1	191	10
471	AT4G33250.1	187	11
472	AT4G33370.1	82	6
473	AT4G33650.1	116	8
474	AT4G34450.1	364	12
475	AT4G34555.1	168	9
476	AT4G34620.1	86	5
477	AT4G34670.1	125	7
478	AT4G35090.1	302	16
479	AT4G35100.1	128	2
480	AT4G35800.1	143	15
481	AT4G36130.1	218	9
482	AT4G37130.1	119	3
483	AT4G37980.1	74	1
484	AT4G38750.1	142	8
485	AT4G38760.1	79	6
486	AT4G38780.1	993	75
487	AT4G39200.1	201	8
488	AT4G39960.1	198	10
489	AT4G40030.1	100	18
490	AT5G01530.1	224	7
491	AT5G02450.1	109	5
492	AT5G02490.1	247	14
493	AT5G02500.1	257	16
494	AT5G02560.1	120	4
495	AT5G02570.1	106	3
496	AT5G02610.1	135	7
497	AT5G02870.1	581	30
498	AT5G02940.1	205	6
499	AT5G02960.1	104	2
500	AT5G03650.1	923	48
501	AT5G04990.1	425	21
502	AT5G06870.1	79	4
503	AT5G06970.1	189	13
504	AT5G08180.1	91	3
505	AT5G08670.1	283	15
506	AT5G09510.1	105	5
507	AT5G09590.1	66	9
508	AT5G09660.1	275	9
509	AT5G09810.1	168	10
510	AT5G09860.1	150	12
511	AT5G10160.1	515	19
512	AT5G10360.1	94	5
513	AT5G10450.1	65	4
514	AT5G10950.1	73	2
515	AT5G11060.1	87	5
516	AT5G11240.1	168	12
517	AT5G13490.1	106	4
518	AT5G13510.1	82	6
519	AT5G14040.1	72	7
520	AT5G14170.1	136	8
521	AT5G14320.1	302	16
522	AT5G14430.1	70	7
523	AT5G14520.1	90	3
524	AT5G14740.1	78	3
525	AT5G14910.1	155	3
526	AT5G15200.1	113	4
527	AT5G15520.1	152	11
528	AT5G15550.1	161	10
529	AT5G15610.1	140	7
530	AT5G16130.1	81	2
531	AT5G16750.1	212	13
532	AT5G18380.1	202	9
533	AT5G18620.1	282	21
534	AT5G19770.1	107	4
535	AT5G20290.1	301	7
536	AT5G20630.1	207	12
537	AT5G22060.1	113	8
538	AT5G22330.1	693	29
539	AT5G22650.1	64	2
540	AT5G22880.1	1076	60
541	AT5G23060.1	282	11
542	AT5G23210.1	116	6
543	AT5G23740.1	81	6
544	AT5G24300.1	490	32
545	AT5G24490.1	80	5
546	AT5G24710.1	236	13
547	AT5G25230.1	1143	54
548	AT5G25754.1	370	20
549	AT5G25780.1	604	33
550	AT5G25980.1	266	7
551	AT5G25980.2	3629	184
552	AT5G26000.1	1037	67
553	AT5G26210.1	63	2
554	AT5G26360.1	89	9
555	AT5G26570.1	251	20
556	AT5G26710.1	761	52
557	AT5G27120.1	76	5
558	AT5G27640.1	655	35
559	AT5G27670.1	183	8
560	AT5G27770.1	169	6
561	AT5G27850.1	222	10
562	AT5G28540.1	989	72
563	AT5G28740.1	197	21
564	AT5G30510.1	581	28
565	AT5G35530.1	258	10
566	AT5G35970.1	392	15
567	AT5G37640.1	167	21
568	AT5G38420.1	132	13
569	AT5G39740.1	369	23
570	AT5G40480.1	744	40
571	AT5G40950.1	148	5
572	AT5G41770.1	732	42
573	AT5G42020.1	934	71
574	AT5G42080.1	917	56
575	AT5G43500.1	199	5
576	AT5G43745.1	99	7
577	AT5G44020.1	288	15
578	AT5G44120.3	238	12
579	AT5G44800.1	109	13
580	AT5G45990.1	113	11
581	AT5G46070.1	997	55
582	AT5G46110.1	83	3
583	AT5G46430.1	77	11
584	AT5G47190.1	183	7
585	AT5G47690.1	506	35
586	AT5G47930.1	120	2
587	AT5G48375.1	190	19
588	AT5G48760.1	112	9
589	AT5G49910.1	184	13
590	AT5G51200.1	435	23
591	AT5G51280.1	104	7
592	AT5G52040.1	142	4
593	AT5G52470.1	418	17
594	AT5G52650.1	152	7
595	AT5G53480.1	80	4
596	AT5G54270.1	130	3
597	AT5G54600.1	179	12
598	AT5G54640.1	427	15
599	AT5G54960.1	169	15
600	AT5G55070.1	131	12
601	AT5G55300.1	67	12
602	AT5G55660.1	67	4
603	AT5G55920.1	80	6
604	AT5G56000.1	126	7
605	AT5G56010.1	96	6
606	AT5G56030.1	68	8
607	AT5G56130.1	67	2
608	AT5G56950.1	133	8
609	AT5G58230.1	71	7
610	AT5G59240.1	98	4
611	AT5G59870.1	200	10
612	AT5G59910.1	1228	65
613	AT5G60660.1	86	2
614	AT5G61170.1	94	6
615	AT5G61970.1	115	7
616	AT5G62890.1	203	9
617	AT5G63420.1	641	42
618	AT5G64270.1	407	22
619	AT5G64420.1	80	6
620	AT5G65220.1	418	9
621	AT5G65350.1	83	6
622	AT5G65750.1	76	6
623	AT5G65770.1	717	49
624	AT5G66190.1	439	17
625	AT5G66680.1	180	9
626	AT5G67320.1	180	11
627	AT5G67380.1	107	6
628	AT5G67630.1	580	21
629	ATCG00020.1	233	7
630	ATCG00120.1	228	10
631	ATCG00160.1	174	11
632	ATCG00170.1	546	29
633	ATCG00180.1	418	21
634	ATCG00190.1	360	19
635	ATCG00270.1	245	5
636	ATCG00280.1	215	10
637	ATCG00340.1	148	4
638	ATCG00350.1	109	8
639	ATCG00380.1	307	13
640	ATCG00480.1	616	37
641	ATCG00490.1	798	48
642	ATCG00500.1	232	6
643	ATCG00540.1	110	7
644	ATCG00650.1	100	6
645	ATCG00660.1	69	1
646	ATCG00680.1	500	14
647	ATCG00740.1	122	4
648	ATCG00750.1	68	2
649	ATCG00770.1	246	6
650	ATCG00780.1	461	15
651	ATCG00790.1	60	2
652	ATCG00800.1	622	28
653	ATCG00810.1	175	9
654	ATCG00820.1	84	6
655	ATCG00830.1	221	7
656	ATCG00840.1	109	8
657	ATCG00900.1	244	11
658	ATCG01020.1	63	4
659	ATCG01110.1	130	5
660	ATCG01120.1	167	7

Table 1

The proteins identified in the *A. thaliana* crude nuclear lamina fraction by mass spectrometry.

AGI codes are from TAIR database (http://www.Arabidopsis.org). Scores were calculated by MASCOT. Peptide represents the number of unique peptides matched.

	AGI code	T-DNA insertion ID
1	AT1G07360.1	SALK_142085
2	AT1G09080.1	SAIL_168_C09
3	AT1G14850.1	SAIL_1286_H03
4	AT1G15290.1	SAIL_633_B04
5	AT1G18850.1	SALK_049296
6	AT1G20600.1	SALK_136329
7	AT1G24310.1	SALK_003112
8	AT1G24706.1	SALK_072011
9	AT1G32900.1	SALK_047731
10	AT1G42430.1	SALK_070292
11	AT1G61730.1	SAIL_688_F01
12	AT1G62330.1	SALK_060288
13	AT1G67230.1	SALK_016800
14	AT1G68910.1	SALK_127765
15	AT1G70770.1	SALK_100857.51.50
16	AT1G77180.1	SAIL_856_B09
17	AT1G79150.1	SALK_070109
18	AT2G19480.1	SAIL_373_H11
19	AT2G27170.1	SALK_015308
20	AT2G35960.1	SALK_106288
21	AT2G41620.1	SALK_012389
22	AT3G01060.1	SALK_071775
23	AT3G06400.1	SALK_082046
24	AT3G11660.1	SALK_117543
25	AT3G14120.1	SALK_057244
26	AT3G14120.2	SALK_057244
27	AT3G18890.1	SALK_150392
28	AT3G19120.1	SALK_059990
29	AT3G28720.1	SALK_027378
30	AT3G54670.1	SALK_072034
31	AT3G55760.1	SALK_005823
32	AT3G57150.1	SALK_066691
33	AT3G57350.1	SAIL_94_A05
34	AT4G00270.1	SALK_031530
35	AT4G26110.1	SALK_129398
36	AT4G28080.1	SALK_020337
37	AT4G28200.1	SALK_035072
38	AT4G32910.1	SALK_133369.30.40
39	AT4G38750.1	SAIL_668_F05
40	AT4G38760.1	SALK_004661
41	AT5G02940.1	SALK_014894
42	AT5G06970.1	SALK_122114
43	AT5G09860.1	SAIL_242_H07_SAIL_304_G05
44	AT5G14520.1	SALK_041045
45	AT5G18620.1	SALK_085156
46	AT5G23060.1	SALK_070416.43.85
47	AT5G24710.1	SALK_057365
48	AT5G25754.1	SAIL_308_B12
49	AT5G25980.1	SALK_038730.43.30
50	AT5G25980.2	SALK_038730.43.30
51	AT5G26000.1	SALK_069615.56.00
52	AT5G28540.1	SALK_063999
53	AT5G35970.1	SALK_037000
54	AT5G42020.1	SAIL_1153_D09
55	AT5G44800.1	SAIL_1290_E09
56	AT5G47690.1	SALK_068683
57	AT5G48375.1	SALK_085567.27.20
58	AT5G51200.1	SALK_055559
59	AT5G55920.1	SALK_048299
60	AT5G56950.1	SALK_147448
61	AT5G65770.1	SALK_079288
62	AT5G66680.1	SALK_063253
63	AT3G05060.1	SALK_010402.53.30

Table 2.

The genes selected from the 660 genes listed in Table 1.

AGI codes are from TAIR database (http://www.Arabidopsis.org). T-DNA insertion IDs are from SALK website (http://signal.salk.edu/).

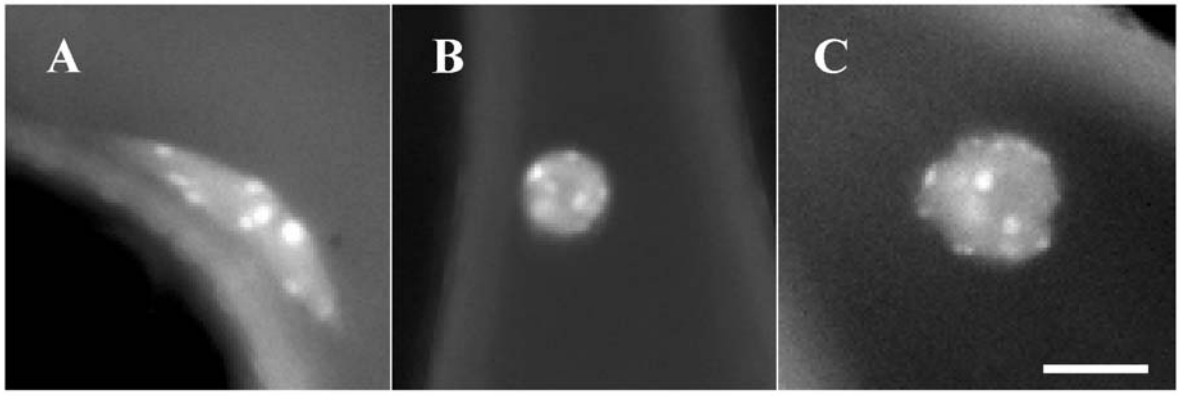

Figure 5

Nuclear morphology of *A.thaliana* gene disruptants of LITTLE NUCLEI 1(LINC1) and LINC4 screened from 63 proteins

Nuclei in trichome cells were visualized by staining the 4-week-old wild-type plants (A), *linc1* disruptants (B), and *linc4* disruptants (C) with Hoechst. The scale bar is 10 μm

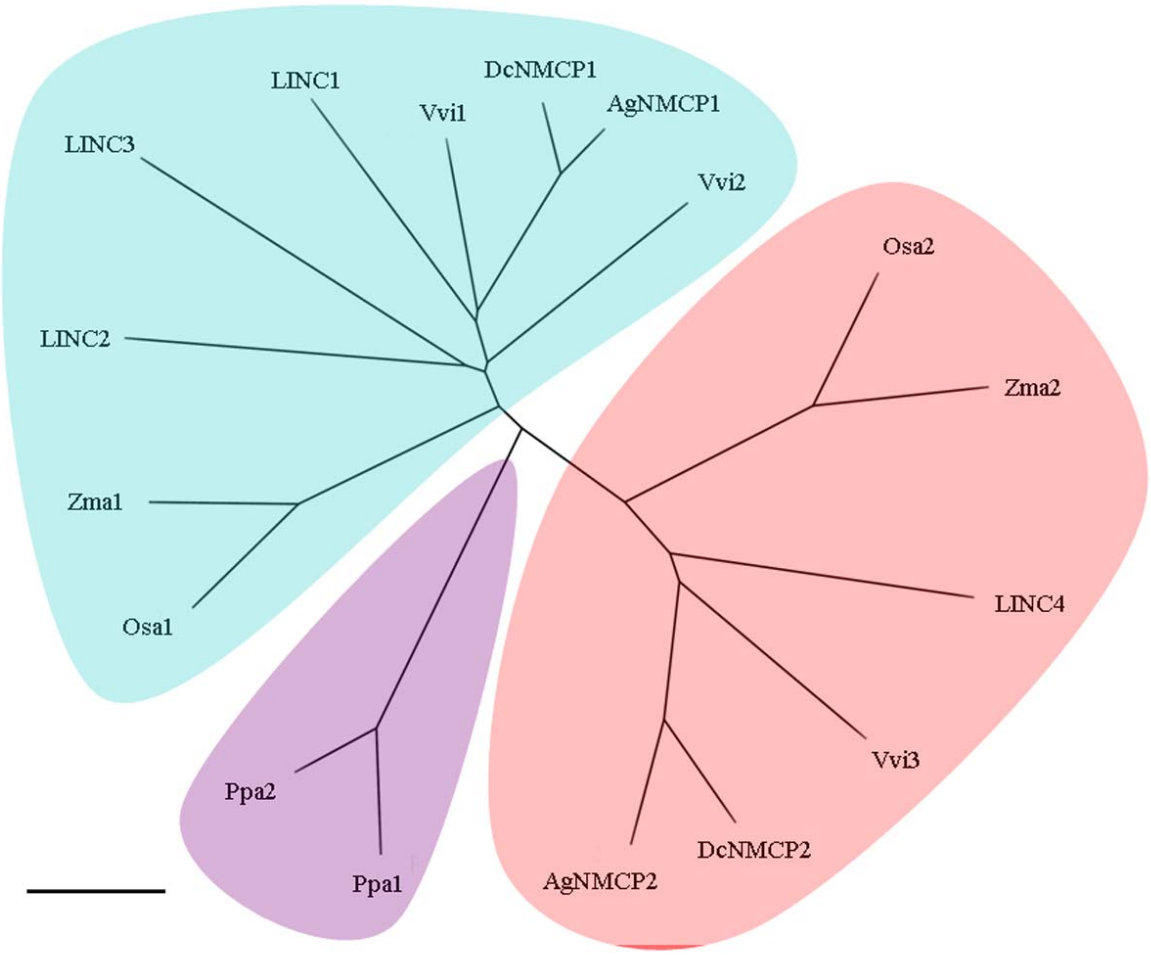

Figure 6

Phylogenetic analysis of LINCs and NMCPs

Blue indicates NMCP1 type, red indicates NMCP2 type, and purple indicates *Physcomitrella patens* special type. Ppa; *Physcomitrella patens* Zma*; Zea mays,* Osa; *Oryza sativa*, Vvi; *Vitis vinifera*, Dc; *Daucus carota*, and Ag; *Apium graveolens*. The scale is 0.1 changes.

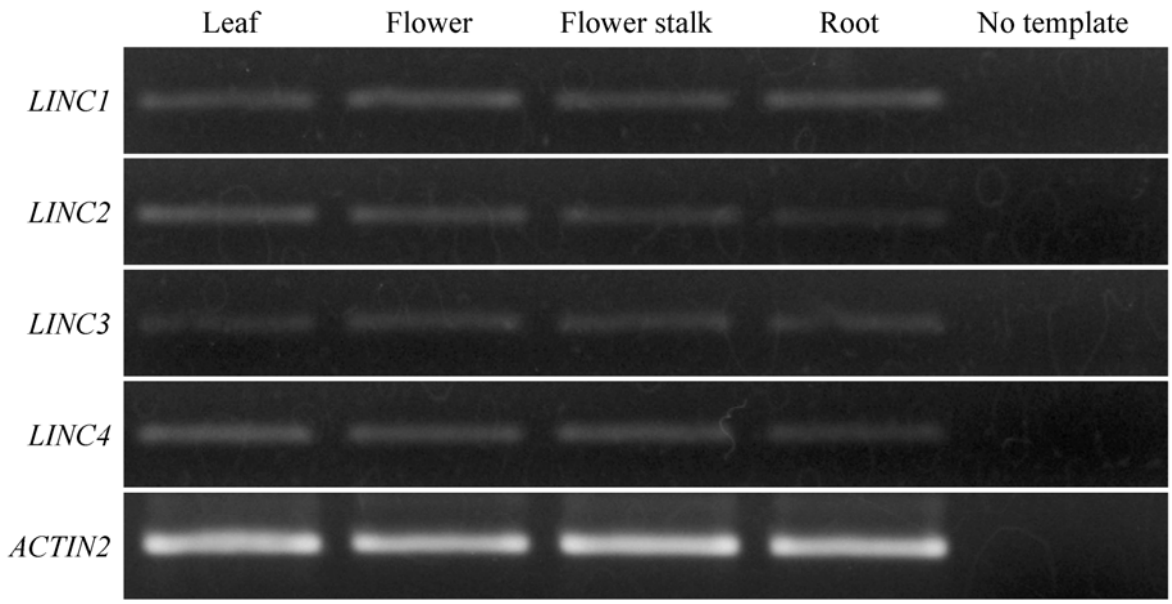

Figure 7

Expression of *LINC* genes in *A. thaliana* wild-type plants

Expression of all *LINC* genes was analyzed in leaves, flowers, flower stalks, and roots of the wild-type plants (WT) by RT-PCR. mRNA was isolated from the 4-week-old plants. *ACTIN2* was used as the internal control.

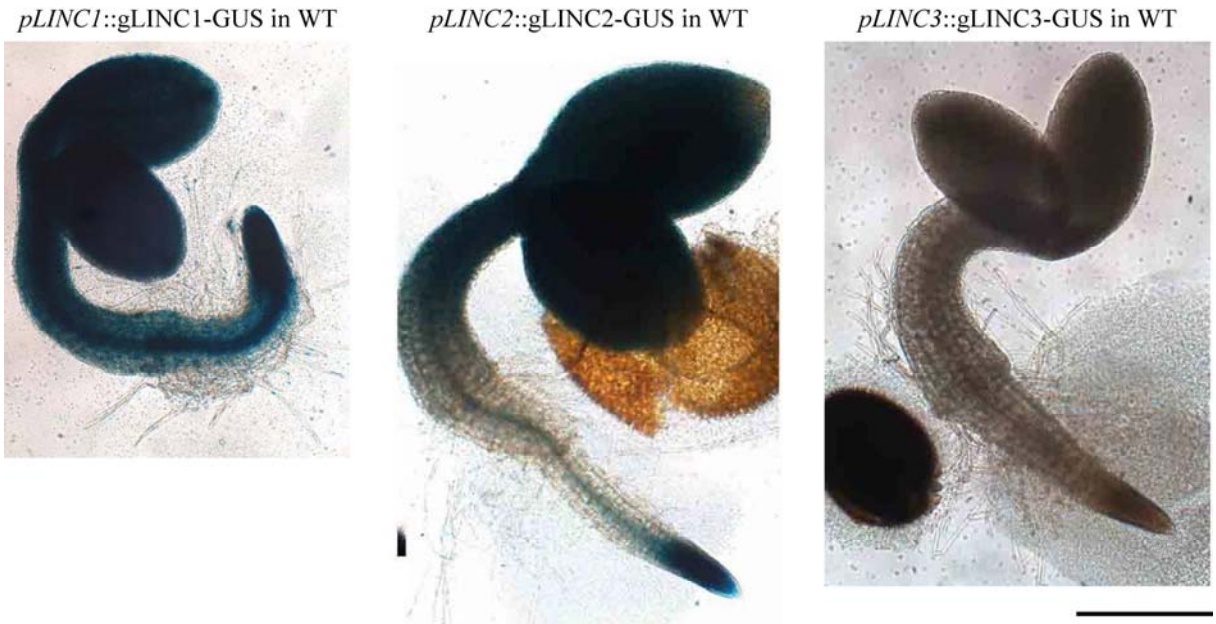

Figure 8

LINC1-LINC3 expression analysis using GUS reporter gene in 2 DAG seedlings of *A. thaliana*

Expression patterns of LINC1-LINC3 in 2 DAG seedlings. The scale bar is 50 μm

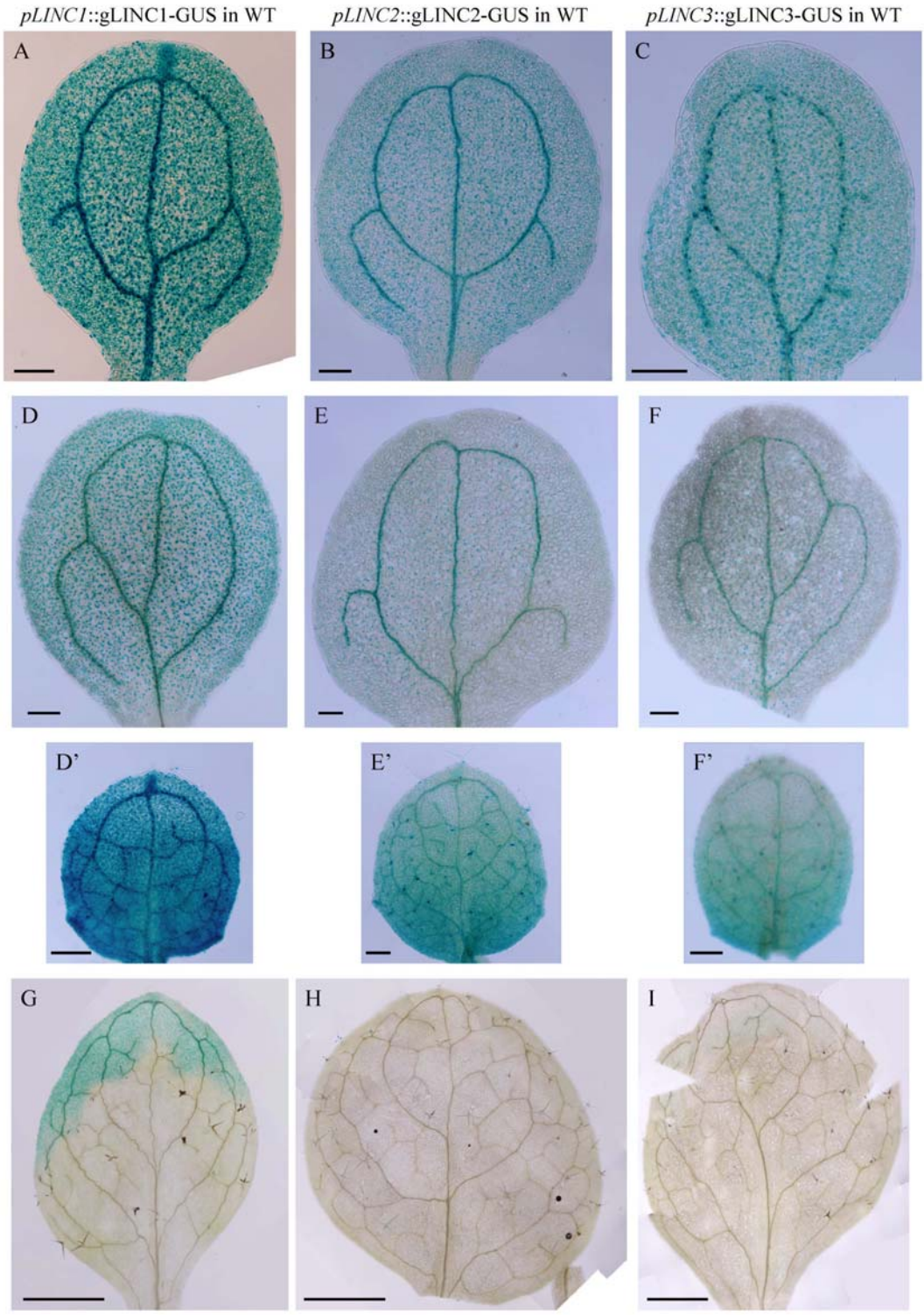

Figure 9

LINC1-LINC3 expression analysis using GUS reporter gene in cotyledons and first true leaves of *A. thaliana*

Expression patterns of LINC1-LINC3 in 5 DAG cotyledons (A, B, C), 8 DAG cotyledons (D, E, F) and first true leaves (D', E', F'), and 14 DAG first true leaves (G, H, I). The scale bars are 200 μm in A-F' and

1 mm in G-I.

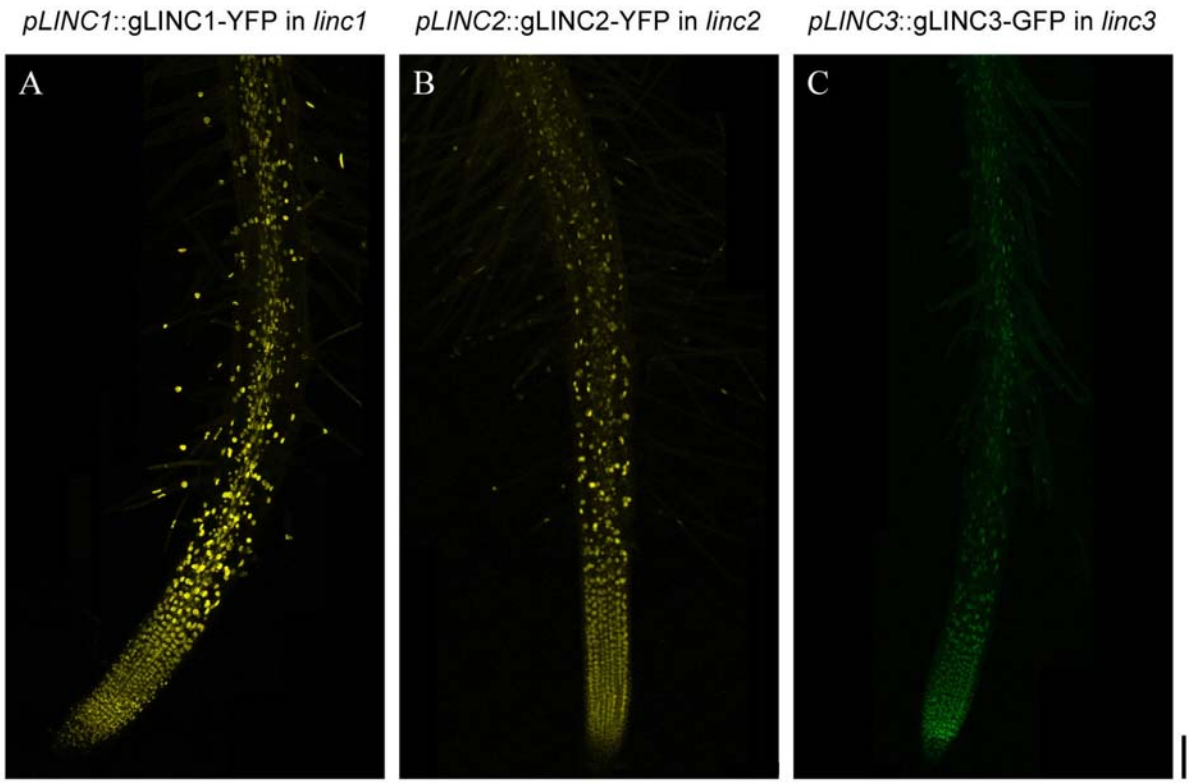

Figure 10

LINC1-LINC3 expression analysis using GFP reporter gene in *A. thaliana* roots

Expression patterns of LINC1-LINC3 in roots. YFP signals are seen yellow, GFP signals are seen green. The scale bar is 100 μm

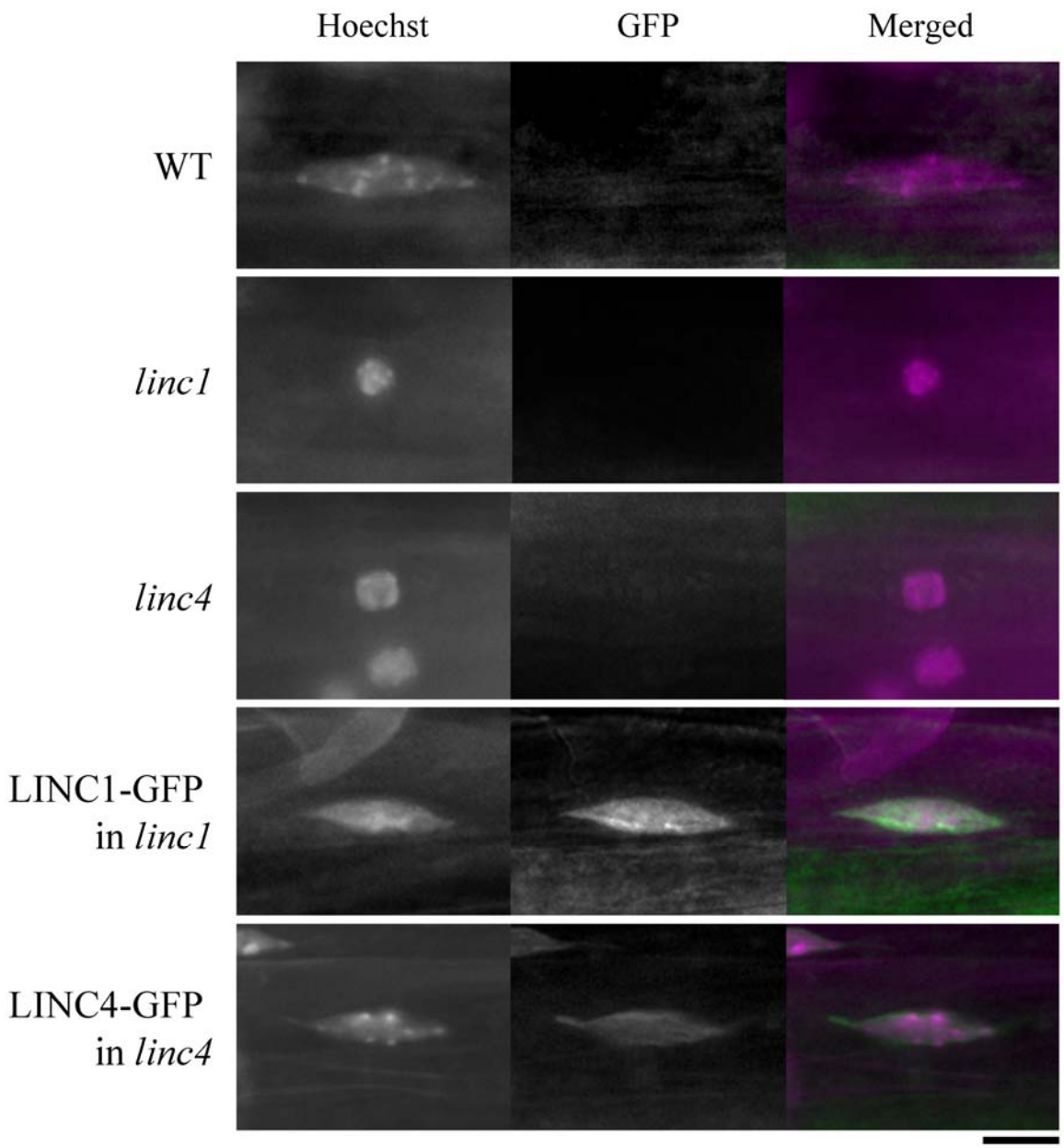

Figure 11

Complementation analysis of LINC1-GFP and LINC4-GFP in *A. thaliana* roots

LINC1-GFP and *LINC4-GFP* driven by a CaMV 35S promoter were transformed into *linc1* and *linc4* disruptants, respectively. Nuclei were observed in root epidermal cells of 2-week-old plants. Hoechst signals are in magenta and GFP signals are in green in the merged images. Scale bar is 10 μm.

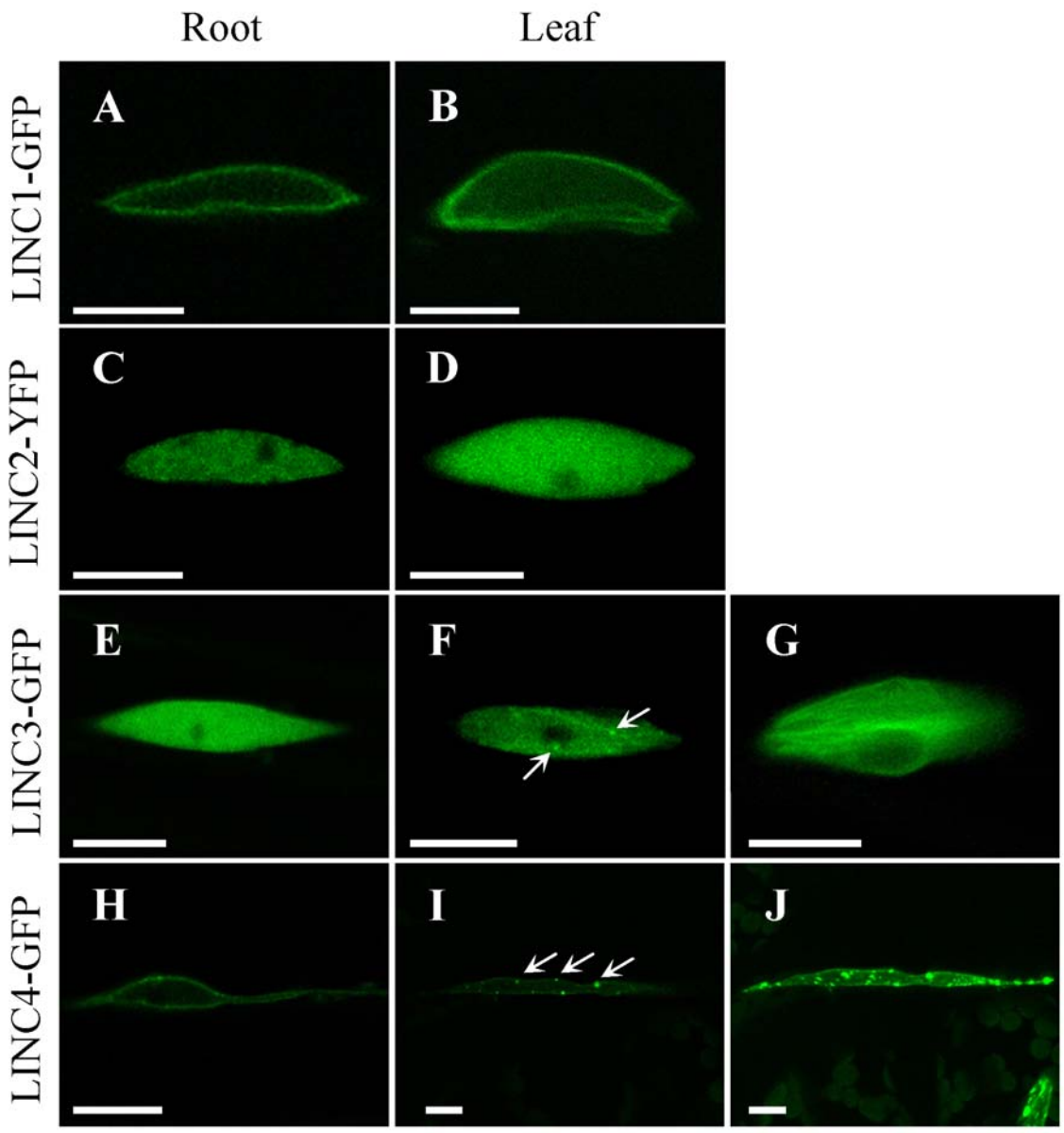

Figure 12

Intracellular localization of LINCs in interphase cells of *A. thaliana*

Localization patterns of LINC1-GFP (A, B), LINC2-YFP (C, D), LINC3-GFP (E, F, G), and LINC4-GFP (H, I, J) were demonstrated in root (A, C, E, H) and leaf epidermal cells (B, D, F, I, J), and trichrome cells (G). (A–I) Confocal section images. (J) Stacked image of confocal sections. (F, I) Arrows indicate GFP signals localized to punctate structures. The scale bars are 10 μm.

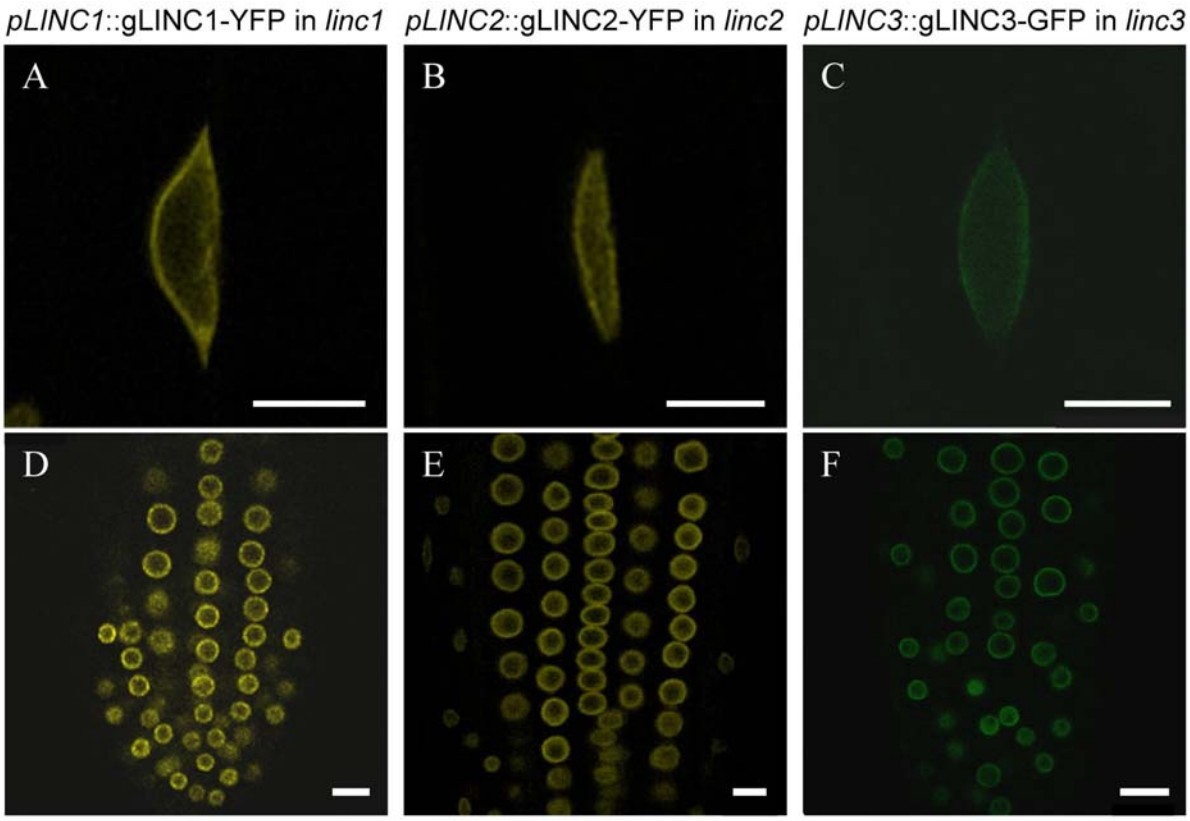

Figure 13

Intracellular localization analysis of LINC1-LINC3 in interphase cells of *A. thaliana* roots

LINC1-LINC3 intracellular localization patterns in differentiated root epidermal cells (A-C) and in root meristematic cells (D-F). Confocal section images (A–F). YFP signals are seen yellow, GFP signals are seen green. The scale bars are 10 μm.

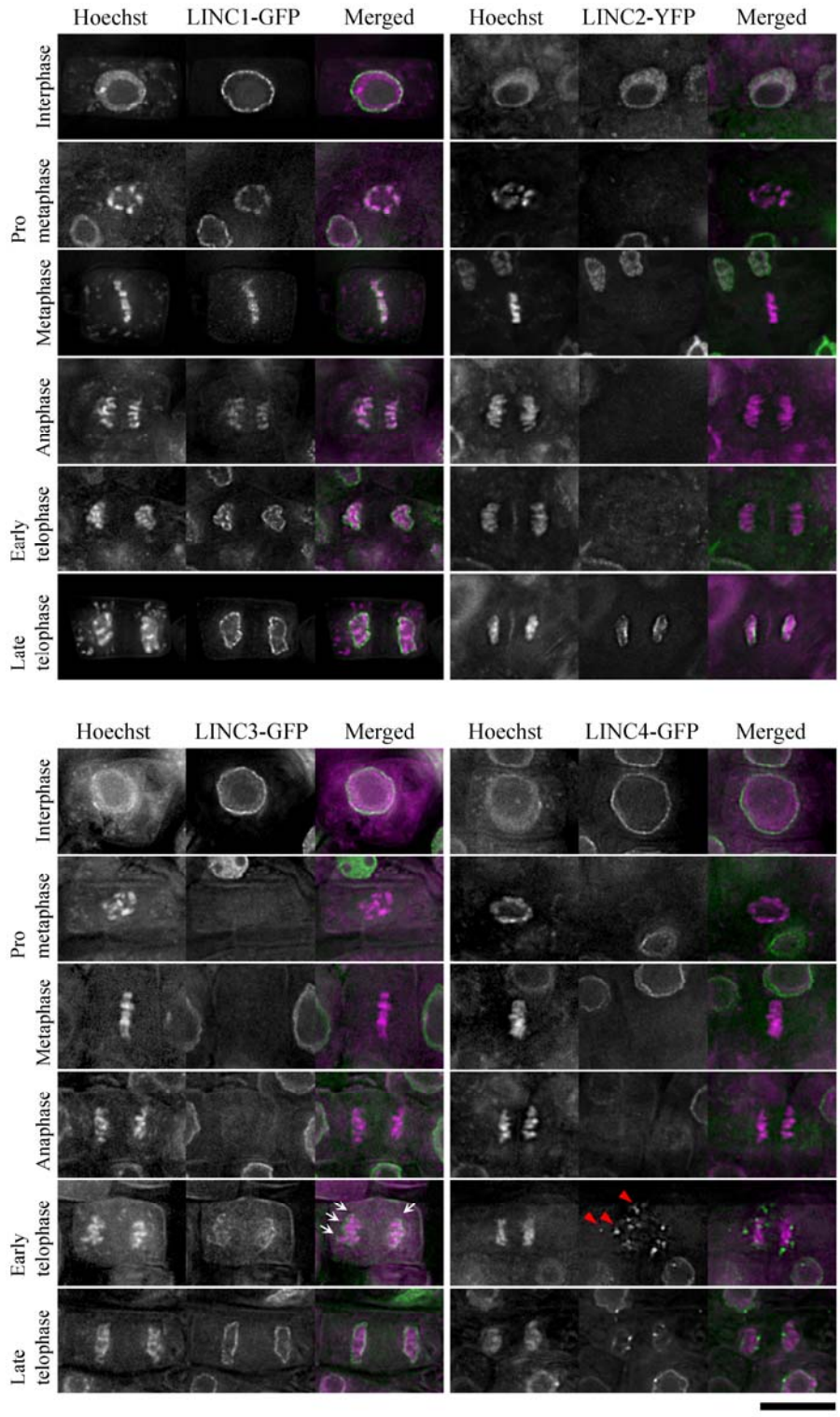

Figure 14

Intracellular localization of LINCs in fixed mitotic cells of *A. thaliana*

Localization patterns of LINC-GFP and -YFP were demonstrated in chemically fixed mitotic root tip cells. Arrows indicate GFP signals localized at the distal surface of chromosomes. Arrow heads indicate GFP signals localized in the cytoplasmic punctate structures. Hoechst signals are in magenta

and GFP and YFP signals are in green in the merged images. Scale bar is 10 μm.

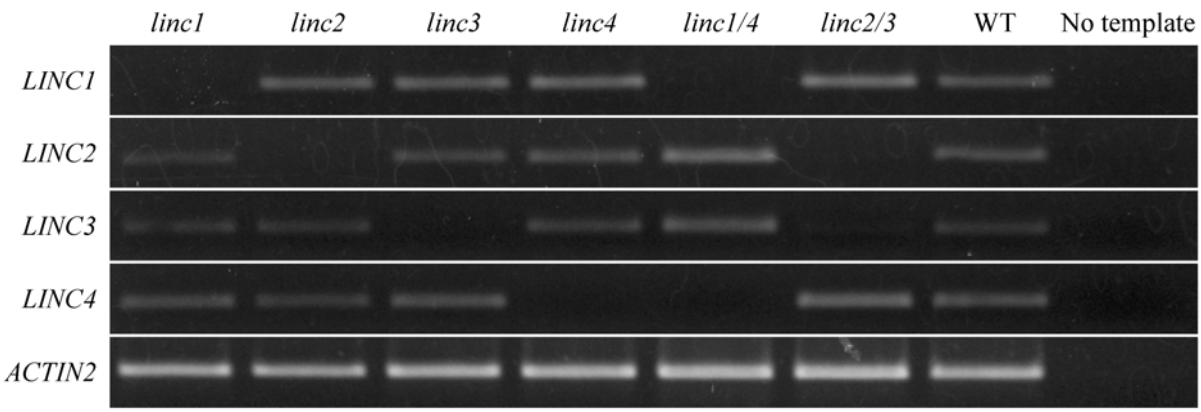

Figure 15

Expression of *LINC* genes in *A. thaliana linc* disruptants

Expression of *LINC* genes was analyzed by reverse transcription polymerase chain reaction (RT-PCR) in the wild-type plants (WT) and *linc* disruptants. mRNA was isolated from the leaves of 4-week-old plants. *ACTIN2* was used as the internal control.

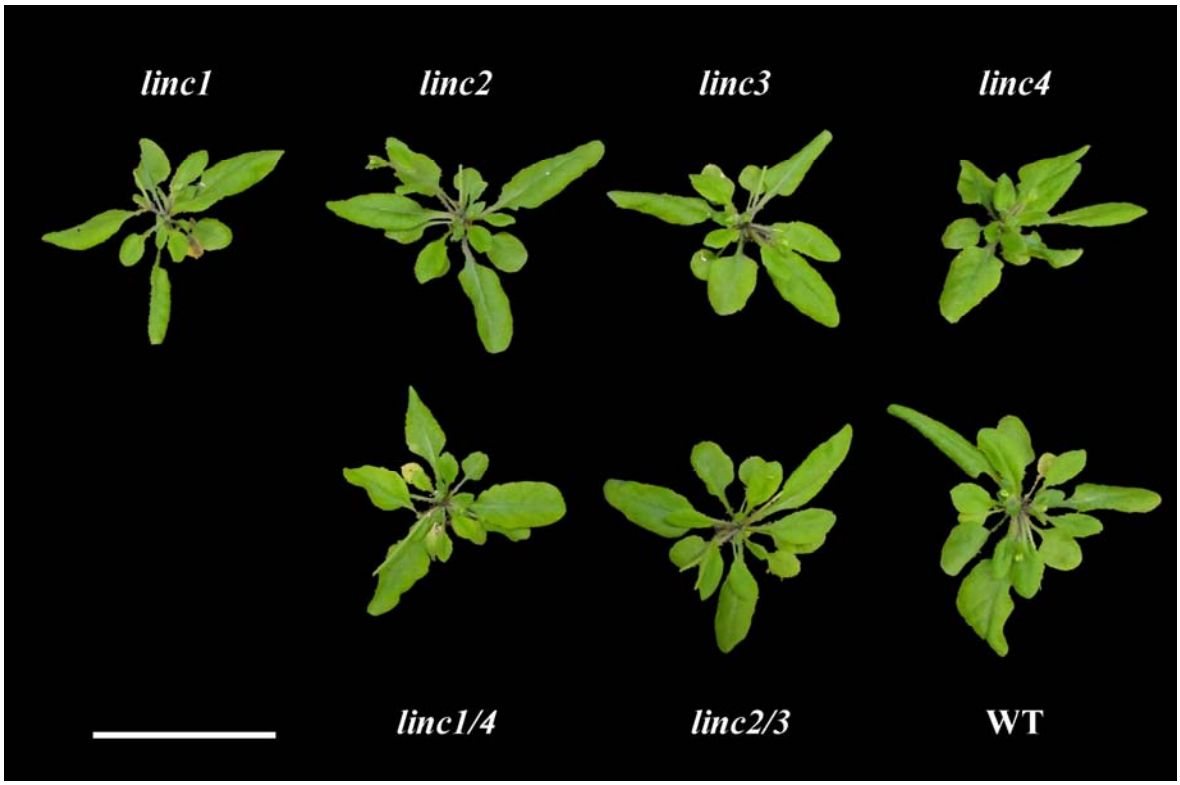

Figure 16

Whole-plant morphology of *A. thaliana linc* disruptants

Representative 4-week-old wild-type plant (WT) and *linc* disruptants are shown. The scale bar is 5 cm.

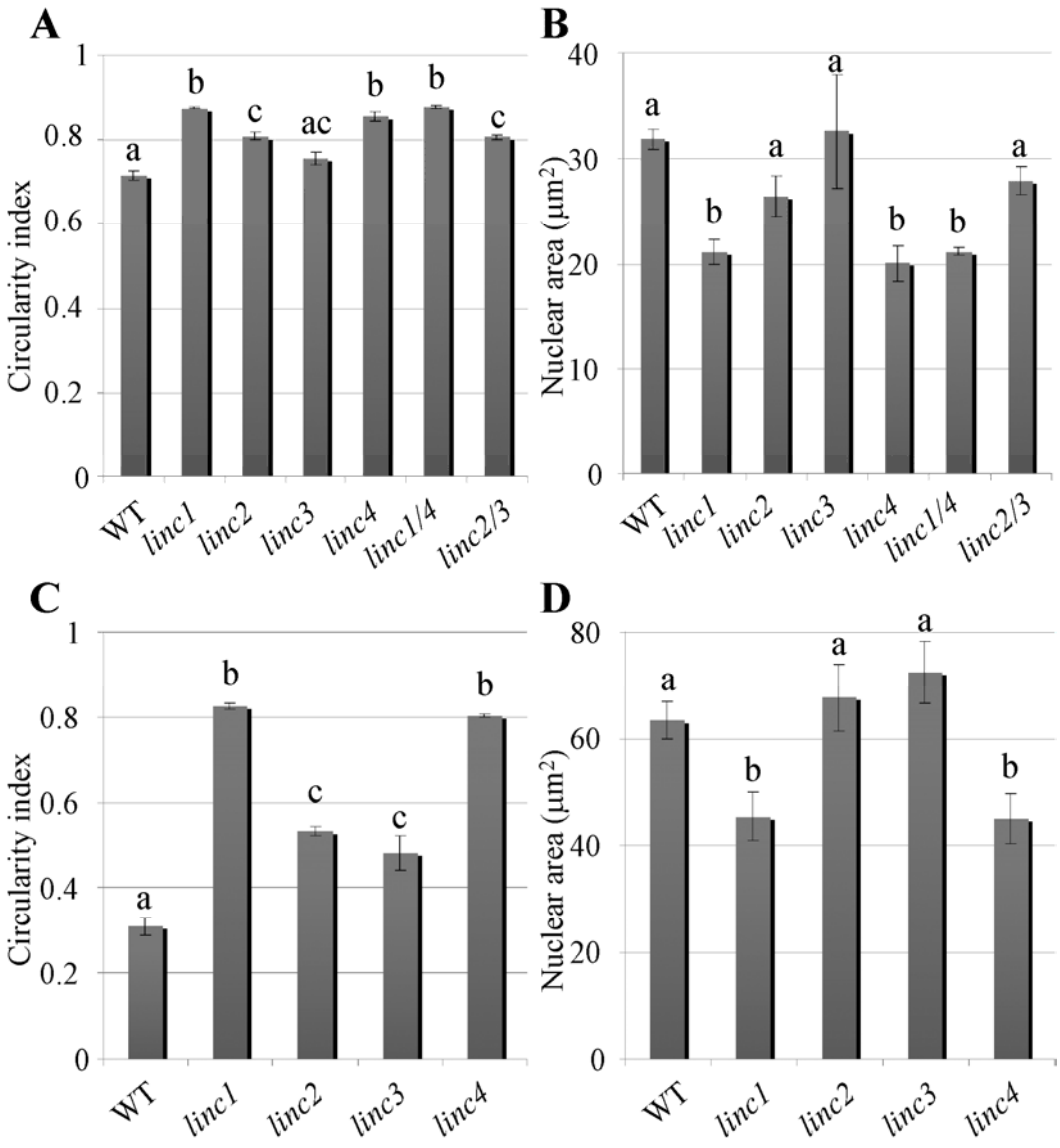

Figure 17

Morphological parameters of nuclei in epidermal cells of *A. thaliana linc* disruptants

The nuclear circularity index (A, C) and nuclear area (B, D) were semi-quantitated from fluorescence images of nuclei stained with Hoechst in the leaf (A, B) and root epidermal cells (C, D) of the wild-type plants (WT) and *linc* disruptants. Different letters indicate a statistical differences detected by Student's *t*-test ($p < 0.05$). More than three different plants and 14–55 nuclei in each were analyzed for each experiment. The vertical bar on each column indicates the standard error.

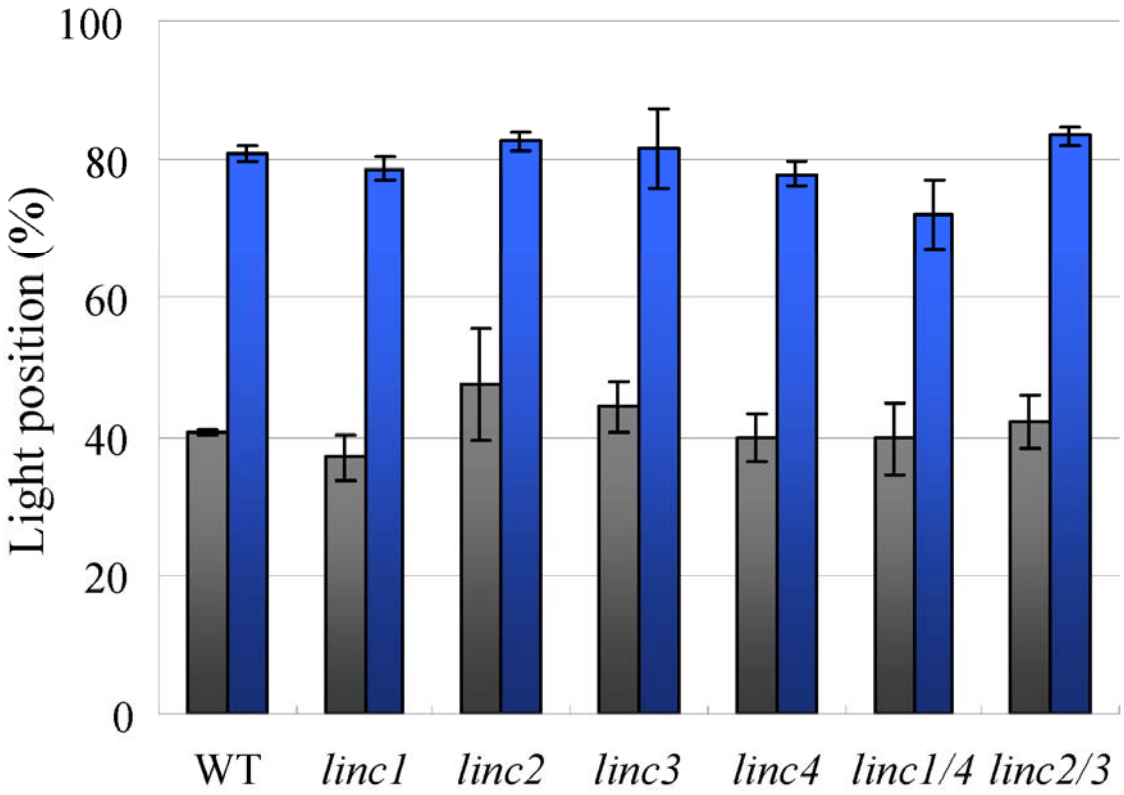

Figure 18

Light-dependent nuclear positioning in *A. thaliana linc* disruptants

Leaves of the wild-type plants (WT) and *linc* disruptants were fixed and stained with Hoechst after dark adaptation for 16 h (black columns) or further exposure to blue light (470 nm, 100 μmol m^{-2} s^{-1}) for 5 h (blue columns). The number of cells in which the nucleus was located along the anticlinal walls was counted and is shown as a percentage. No difference was detected between *linc* disruptants and wild-type plants by Student's *t*-test ($p > 0.05$). Three different plants (>50 cells) were analyzed for each experiment. The vertical bar on each column indicates the standard error.

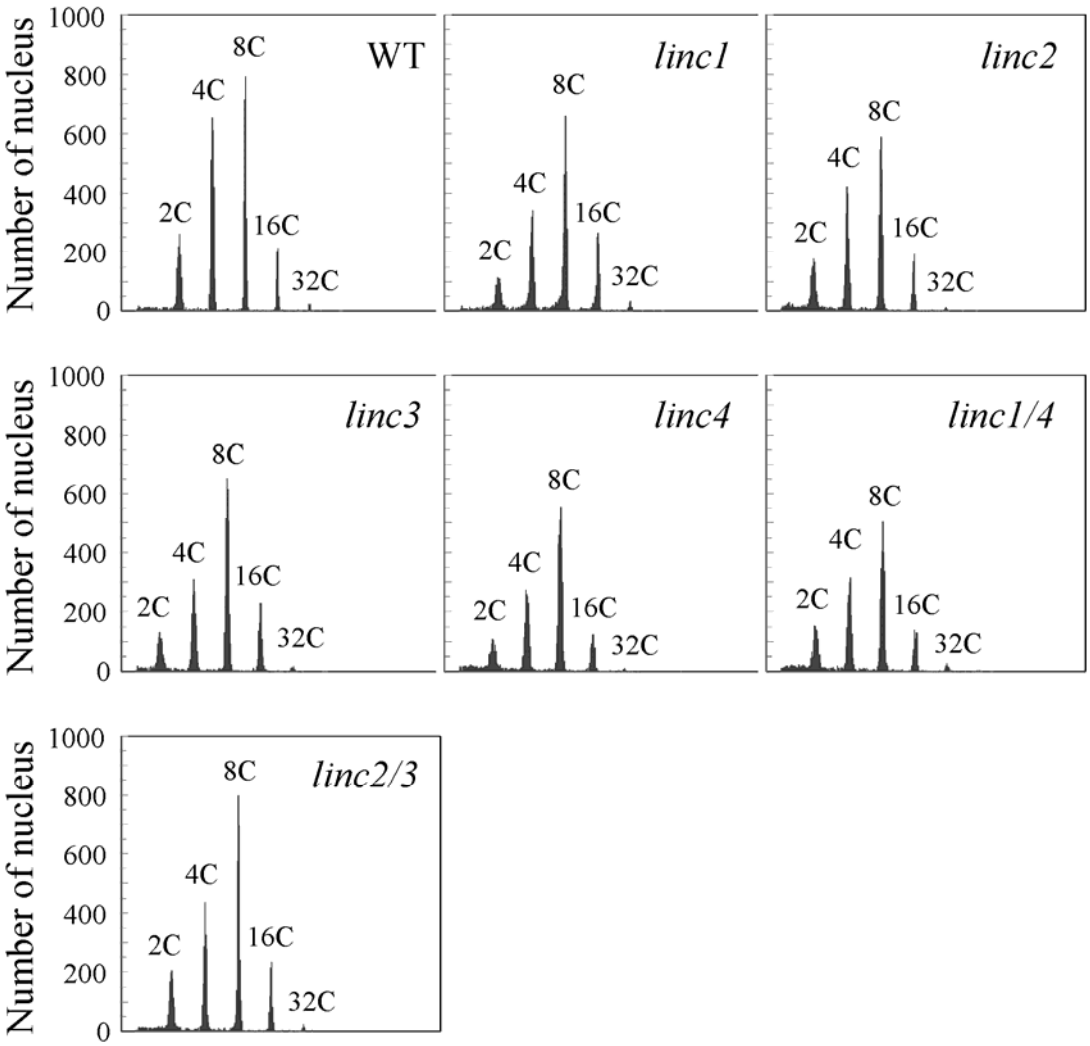

Figure 19

Ploidy level of nuclei isolated from leaves of *A. thaliana linc* disruptants

Isolated nuclei from 4-week-old leaves of the wild-type plants (WT) and *linc* disruptants were analyzed by flow cytometry. More than 7000 nuclei were analyzed in each experiment.

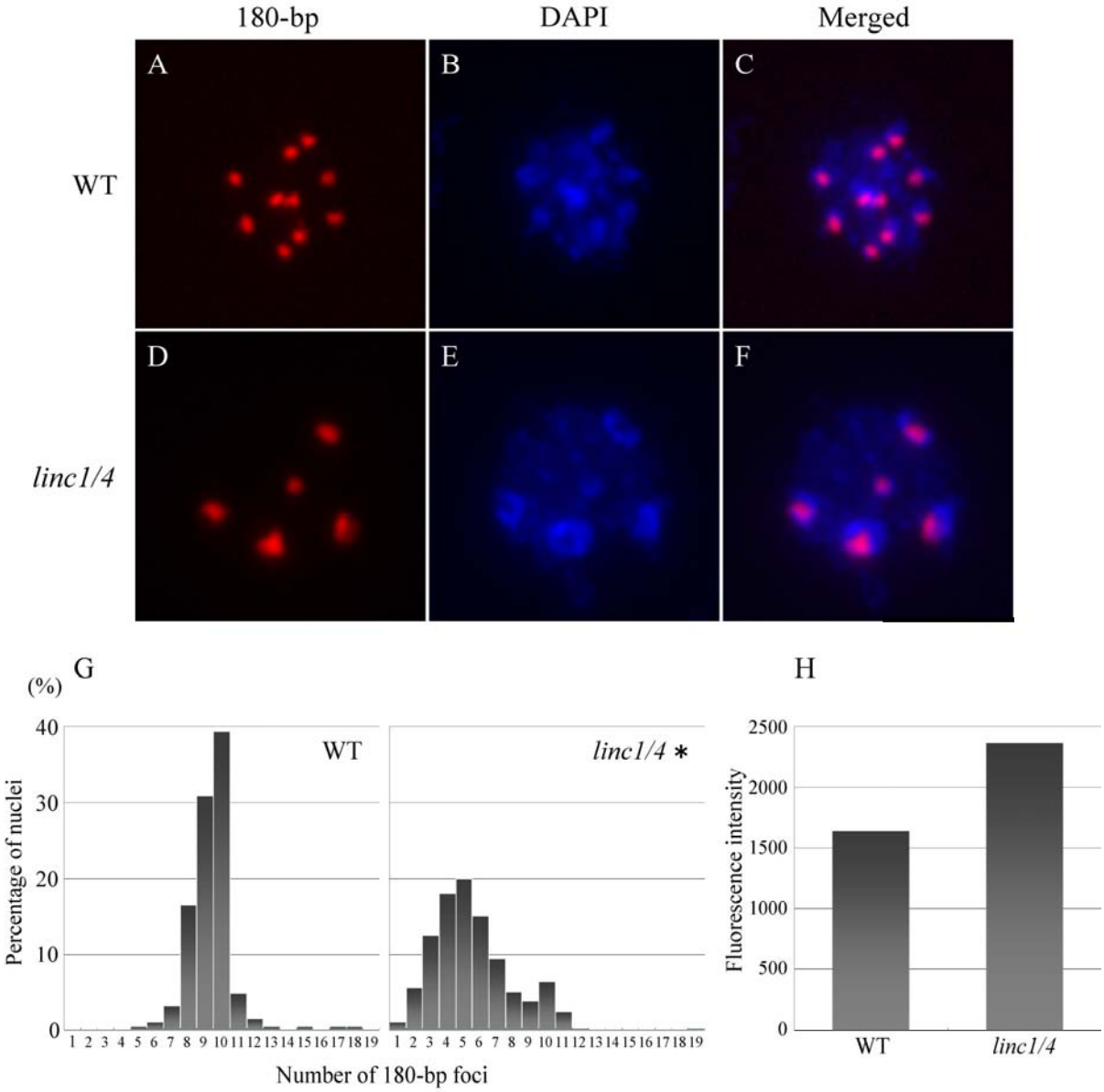

Figure 20

FISH analysis for *A. thaliana linc1/4* disruptants using 180-bp DNA probe

180- bp DNA probe signals are seen red in wild-type plants (A, C) and *linc1/linc4* disruptants (D, F). DAPI signals are seen blue in wild-type plants (B, C) and *linc1/linc4* disruptants (E, F). A number of 180-bp foci per one nucleus was quantified and indicated as histograms (G). Total fluorescence intensity of 180-bp DNA probe signals per one nucleus was analyzed in wild-type plants and *linc1/linc4* disruptants (H). The scale bar is 10 μm. An asterisk indicates a statistical difference detected by χ^2-test ($p < 0.05$).

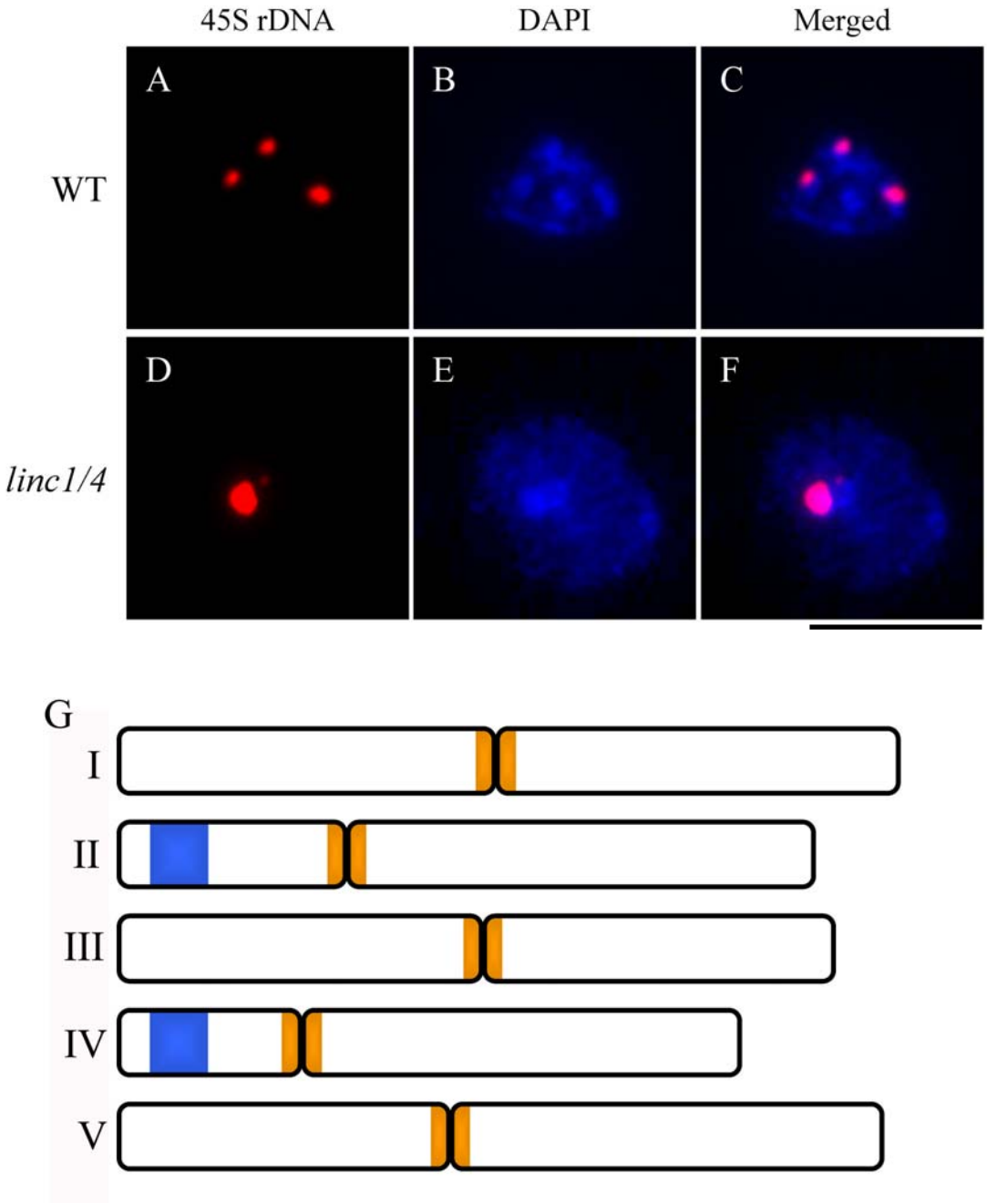

Figure 21

FISH analysis for *A. thaliana linc1/4* disruptants using 45S-rDNA probe and diagram of *A. thaliana* chromosomes

45S-rDNA probe signals are seen red in wild-type plants (A, C) and *linc1/linc4* disruptants (D, F). DAPI signals are seen blue in wild-type plants (B, C) and *linc1/linc4* disruptants (E, F). G is a diagram of *A. thaliana* chromosomes. 180-bp DNA probes recognized orange regions (centromere) and 45S-rDNA probes recognized blue regions. The scale bar is 10 μm.

Acknowledgements

I am grateful to Drs. Keiko Sugimoto and Shinichiro Komaki (RIKEN Plant Science Center, Japan) for technical advice on the flow cytometry, Dr. Sachihiro Matsunaga and Mr. Tomoya Sugiyama (Tokyo University of Science, Japan) for technical advice on the fluorescence in situ hybridization, Drs. Yoichiro Fukao and Masayuki Fujiwara (NAIST, Japan) for technical advice on the LC-MS/MS analysis, Dr. Satoshi Fujii (Osaka University, Japan) for technical advice on the electron microscopy, Dr. Tatsuo Kakimoto and Yasushi Shimizu (Osaka University, Japan) for providing the binary vectors, Dr. Tsuyoshi Nakagawa (Shimane University, Japan) for providing the pGWB vectors, and Dr. Shinobu Takada (Osaka University, Japan) for technical advice on gene cloning. I would express my gratitude to present my laboratory members, Dr. Yuki Sakai, Dr. Kosei Iwabuchi (Kyoto University, Japan), and Dr. Takashi Hotta (NAIST, Japan).

Finally, I would like to express my greatest gratitude to Dr. Shingo Takagi my mentor. He discussed experimental and personal problems with me whenever I want. If there was not his advice, I was not able to achieve my study and student life.

References

Al-Haboubi, T., Shumaker, D.K., Köser, J., Wehnert, M., Fahrenkrog, B. (2011) Distinct association of the nuclear pore protein Nup153 with A- and B-type lamins. Nucleus 2: 500–509

Arango, M., Gévaudant, F., Oufattole, M., Boutry, M. (2003) The plasma membrane proton pump ATPase: the significance of gene subfamilies. Planta 216: 355–365

Baye, L.M., Link, B.A. (2008) Nuclear migration during retinal development. Brain. Res. 1192: 29–36

Bennett,M.D. (1984) Nuclear Architecture and Its Manipulation. Stadler Genetics Symposium 469-502

Burgos M., Fawcett D. (1956) An electron microscope study of spermatid differentiation in the toad, Bufo arenarum Hensel. J. Biophys. Biochem. Cytol. 2: 223–240

Burke, B., Ellenberg, J. (2002) Remodelling the walls of the nucleus. Nat. Rev. Mol. Cell Biol. 3: 487–497

Chytilova, E., Macas, J., Galbraith, D. (1999) Green fluorescent protein targeted to the nucleus, a transgenic phenotype useful for studies in plant biology. Ann. Bot. 83: 645–654

Chytilova, E., Macas, J., Sliwinska, E., Rafelski, S.M., Lambert, G.M., Galbraith, D.W. (2000) Nuclear dynamics in Arabidopsis thaliana. Mol. Biol. Cell 11: 2733-2741

Ciska, M., Masuda, K., Moreno Diaz de la Espina, S. (2013) Lamin-like analogues in plants: the characterization of NMCP1 in Allium cepa. J.Exp.Bot. online

Cremer, T., Cremer, C. (2001) Chromosome territories, nuclear architecture and gene regulation in mammalian cells. Nat Rev Genet. 2(4):292-301.

Dadoune, J.P. (1995) The nuclear status of human sperm cells. Micron 26: 323–345

Dechat, T., Pfleghaar, K., Sengupta, K., Shimi, T., Shumaker, D.K., Solimando, L. et al. (2008) Nuclear lamins: major factors in the structural organization and function of the nucleus and chromatin. Genes Dev. 22: 832–53

Dessev, G., Goldman, R. (1988) Meiotic breakdown of nuclear envelope in oocytes of Spisula solidissima involves phosphorylation and release of nuclear lamin. Dev. Biol. 130: 543–550

Dessev, G., Iovcheva, C., Tasheva, B., Goldman, R. (1988) Protein kinase activity associated with the nuclear lamina. Proc. Natl. Acad. Sci. USA. 85: 2994–2998

Dessev, G., Palazzo, R., Rebhun, L., Goldman, R. (1989) Disassembly of the nuclear envelope of spisula oocytes in a cell-free system. Dev. Biol. 131: 496–504

Dessev, G., Iovcheva-Dessev, C., Goldman, R. (1990) Lamin dimers. Presence in the nuclear lamina of surf clam oocytes and release during nuclear envelope breakdown. J. Biol. Chem. 265: 12636–12641

Dittmer, T.A., Stacey, N.J., Sugimoto-Shirasu, K., Richards, E.J. (2007) LITTLE NUCLEI genes affecting nuclear morphology in Arabidopsis thaliana. Plant Cell 19: 2793–2803

Dittmer, T., Richards, E. (2008) Role of LINC proteins in plant nuclear morphology. Plant Signal. Behav. 3: 485–487

Duckett, J.G., Ligrone, R. (1995) The formation of catenate foliar gemmae and the origin of oil bodies in the liverwort Odontoschisma denudatum (Mart). Dum. Jungermmaniales: a light and electron microscope study. Ann. Bot. 76:405–419.

Ellenberg, J., Siggia, E.D., Moreira, J.E., Smith, C.L., Presley, J.F., Worman, H.J. et al. (1997) Nuclear membrane dynamics and reassembly in living cells: targeting of an inner nuclear membrane protein in interphase and mitosis. J. Cell Biol. 138: 1193–1206

Evans, D.E., Shvedunova, M., Graumann, K. (2011) The nuclear envelope in the plant cell cycle: structure, function and regulation. Ann. Bot. 107: 1111–1118

Fujimoto, S., Ito, M., Matsunaga, S., Fukui, K. (2005) An upper limit of the ratio of DNA volume to nuclear volume exists in plants. Genes Genet. Syst. 80: 345–350

Fujiwara, M.T., Hamada, S., Hiratsuka, M., Fukao, Y., Kawasaki, T., Shimamoto, K. (2009) Proteome Analysis of Detergent-Resistant Membranes (DRMs) Associated with OsRac1-Mediated Innate Immunity in Rice. Plant Cell Physiol. 50: 1191–1200

Gerlich, D., Beaudouin, J., Kalbfuss, B., Daigle, N., Eils, R., Ellenberg, J. (2003) Global chromosome positions are transmitted through mitosis in mammalian cells. Cell. 112(6):751-764.

Gindullis, F., Peffer, N.J., Meier, I. (1999) MAF1, a novel plant protein interacting with matrix attachment region binding protein MFP1, is located at the nuclear envelope. Plant Cell 11: 1755–1768

Gomes, E.R., Jani, S., Gundersen, G.G. (2005) Nuclear movement regulated by Cdc42, MRCK, myosin, and actin flow establishes MTOC polarization in migrating cells. Cell 121: 451–463

Güttinger, S., Laurell, E., Kutay, U. (2009) Orchestrating nuclear envelope disassembly and reassembly during mitosis. Nat. Rev. Mol. Cell Biol. 10: 178–191

Graumann, K., Evans, D. (2011) Nuclear envelope dynamics during plant cell division suggest common mechanisms between kingdoms. Biochem. J. 667: 661–667

Heslop-Harrison, J., Heslop-Harrison, Y. (1989) Conformation and movement of the vegetative nucleus of the angiosperm pollen tube: association with the act in cytoskeleton. J. Cell Sci. 93: 299-308

Hetzer, M.W. (2010) The nuclear envelope. Cold Spring Harb. Perspect. Biol. 2: a000539

Hirano, T., Hoshino, Y. (2010) Sperm dimorphism in terms of nuclear shape and microtubule accumulation in Cyrtanthus mackenii. Sex. Plant Reprod. 23: 153–162

Hoffmann, K., Dreger, C., Olins, A., Olins, D., Shultz, L., Lucke, B., Karl, H., Kaps, R., Muller, D., Vaya, A., Anzar, J., Ware, R., Cruz, N. S., Lindner, T. H., Herrmann, H., Reis, A., Sperling, K. (2002) Mutations in the gene encoding the lamin B receptor produce an altered nuclear morphology in granulocytes (Pelger–Hue¨tanomaly). Nature Genetics, 31, 410–414.

Hoffmann, K., Sperling, K., Olins, A.L., Olins, D.E. (2007) The granulocyte nucleus and lamin B receptor: avoiding the ovoid. Chromosoma 116: 227–235

Hotta, T., Haraguchi, T., Mizuno, K. (2007) A novel function of plant histone H1: microtubule nucleation and continuous plus end association. Cell Struct. Funct. 32: 79–87

Irons, S.L., Evans, D.E., Brandizzi, F. (2003) The first 238 amino acids of the human lamin B receptor are targeted to the nuclear envelope in plants. J. Exp. Bot. 54: 943–950

Ishida, T., Kurata, T., Okada, K., Wada, T. (2008) A genetic regulatory network in the development of trichomes and root hairs. Annu. Rev. Plant Biol. 59: 365–386

Iwabuchi, K., Sakai, T., Takagi, S. (2007) Blue light-dependent nuclear positioning in Arabidopsis thaliana leaf cells. Plant Cell Physiol. 48: 1291–1298

Iwabuchi, K., Minamino, R., Takagi, S. (2010) Actin Reorganization Underlies Phototropin-Dependent Positioning of Nuclei in Arabidopsis Leaf Cells. Plant Physiol. 152: 1309–1319

Jefferson, R.A., Kavanagh, T.A., Bevan, M.W. (1987) GUS fusions: beta-glucuronidase as a sensitive and versatile gene fusion marker in higher plants. EMBO J. 6 (13):3901-3907.

Jovtchev, G., Schubert, V., Meister, A., Barow, M., Schubert, I. (2006) Nuclear DNA content and nuclear and cell volume are positively correlated in angiosperms. Cytogenet. Genome Res.114: 77–82

Khatau, S.B., Hale, C.M., Stewart-Hutchinson, P.J., Patel, M.S., Stewart, C.L., Searson, P.C. et al. (2009) A perinuclear actin cap regulates nuclear shape. Proc. Natl. Acad. Sci. USA. 106: 19017–19022

Ketelaar, T., Faivre-Moskalenko, C., Esseling, J.J., de Ruijter, N.C., Grierson, C.S., Dogterom, M., Emons, A.M. (2002) Positioning of nuclei in Arabidopsis root hairs: an actin-regulated process of tip growth. Plant Cell 14: 2941-2955

Kimura, Y., Kuroda, C., Masuda, K. (2010) Differential nuclear envelope assembly at the end of mitosis in suspension-cultured Apium graveolens cells. Chromosoma 119: 195–204

Křeček, P., Skůpa, P., Libus, J., Naramoto, S., Tejos, R., Friml, J. et al. (2009) The PIN-FORMED (PIN) protein family of auxin transporters. Genome Biol. 10: 249

Ligrone, R., Duckett, J.G. (1994) Cytoplasmic polarity and endoplasmic microtubules associated with the nucleus and organelles are ubiquitous features of food-conducting cells in bryalean mosses (Bryophyta). New Phytologist. 127:601–604.

Lu, Q., Tang, X., Tian, G., Wang, F., Liu, K., Nguyen, V. et al. (2010) Arabidopsis homolog of the yeast TREX-2 mRNA export complex: components and anchoring nucleoporin. Plant J. 61: 259–270

Lüke, Y., Zaim, H., Karakesisoglou, I. (2008) Nesprin-2 Giant (NUANCE) maintains nuclear envelope architecture and composition in skin. J. Cell Sci. 121: 1887–1898

Luxton, G.W.G., Gomes, E.R., Folker, E.S., Vintinner, E., Gundersen, G.G. (2010) Linear arrays of nuclear envelope proteins harness retrograde actin flow for nuclear movement. Science 329: 956–959

Manuelidis, J., Borden, L. (1988) Movement of the X Chromosome in Epilepsy. Science 242: 1687-1691

Masuda, K., Xu, Z.J., Takahashi, S., Ito, A., Ono, M., Nomura, K. et al. (1997) Peripheral framework of carrot cell nucleus contains a novel protein predicted to exhibit a long alpha-helical domain. Exp. Cell Res. 232: 173–181

Masuda, K., Haruyama, S. (1999) Assembly and disassembly of the peripheral architecture of the plant cell nucleus during mitosis. Planta 210(1): 165–167

Meier, I. (2007). Composition of the plant nuclear envelope: Theme and variations. J. Exp. Bot. 58: 27–34.
Murata M., Heslop-Harrison J.S., Motoyoshi F.(1997) Physical mapping of the 5S ribosomal RNA genes in Arabidopsis thaliana by multi-color fluorescence in situ hybridization with cosmid clones. Plant J. 12: 31-37

McNulty, A. K., Saunders, M.J. (1992) Purification and immunological detection of pea nuclear intermediate filaments: evidence for plant nuclear lamins. J. Cell Sci. 103: 407–414

Melaragno, J.E., Mehrotra, B., Coleman, A.W. (1993) Relationship between Endopolyploidy and Cell Size in Epidermal Tissue of Arabidopsis. Plant Cell 5: 1661–1668

Nakagawa, T., Suzuki, T., Murata, S., Nakamura, S., Hino, T., Maeo, K. et al. (2007) Improved Gateway Binary Vectors: High-Performance Vectors for Creation of Fusion Constructs in Transgenic Analysis of Plants. Biosci. Biotechnol. Biochem. 71: 2095–2100

Nakayama, T., Ishii, T., Hotta, T., Mizuno, K. (2008) Radial microtubule organization by histone H1 on nuclei of cultured tobacco BY-2 cells. J. Biol. Chem. 283: 16632–16640

Oda, Y., Fukuda, H. (2011) Dynamics of Arabidopsis SUN proteins during mitosis and their involvement in nuclear shaping. Plant J. 66: 629–641

Ojangu, E., Tanner, K., Pata, P., Jarve, J., Holweg, C. Truve, E., Paves, H. (2012) Myosins XI-K, XI-1, and XI-2 are required for development of pavement cells, trichomes, and stigmatic papillae in Arabidopsis. BMC Plant Boil. 12: 81-97

Olins, A.L., Olins, D.E. (2004) Cytoskeletal influences on nuclear shape in granulocytic HL-60 cells. BMC Cell Boil. 5: 30

Palmgren, M.G. (2001) PLANT PLASMAMEMBRANEH^+-ATPases: Powerhouses for Nutrient Uptake. Annu. Rev. Plant Physiol. Plant Mol. Biol. 52: 817–845

Paolillo, D.J., Kreitner, G.L., Reighard, J.A. (1984a) Spermatogenesis in Polytrichum juniperinum. Planta 78 226-247

Paolillo, D.J., Kreitner, G.L., Reighard, J.A. (1984b) Spermatogenesis in Polytrichum juniperinum. Planta 78 248-261

Prekins, D.N., Pappin, D.J.C., Creasy, D.M., Cottrell, J.S. (1999) Probability-based protein identification by searching sequence databases using mass spectrometry data. Electrophoresis 20: 3551–3567

Pressel, S., Ligrone, R., Duckett, J.G. (2008) Cellular differentiation in moss protonemata: a morphological and experimental study. Ann. Bot. 102: 227-245

Rose, A., Gindullis, F., Meier, I. (2003) A novel alpha-helical protein, specific to and highly conserved in plants, is associated with the nuclear matrix fraction. J. Exp. Bot. 54: 1133–1141

Sakamoto,T., Tsujimoto Inui, Y., Uraguchi,S., Yoshizumi,T., Matsunaga,S., Mastui,M., Umeda,M., Fukui,K., Fujiwara,T. (2011) Condensin II Alleviates DNA Damage and Is Essential for Tolerance of Boron Overload Stress in Arabidopsis. Plant Cell 23: 3533-3546

Schubert,V., Lermontova,I., Schubert,I. (2013) The Arabidopsis CAP-D proteins are required for correct chromatin organisation, growth and fertility. Chromosoma In press

Shimi, T., Butin-Israeli, V., Adam, S.A., Goldman, R.D. (2010) Nuclear lamins in cell regulation and disease. Cold Spring Harb. Symp. Quant. Biol. 75: 525–531

Sieberer, B.J., Timmers, A.C., Lhuissier, F.G., Emons, A.M. (2002) Endoplasmic microtubules configure the subapical cytoplasm and are required for fast growth of Medicago truncatula root hairs. Plant Physiol. 130: 977-988

Smythe, C., Jenkins, H.E., Hutchison, C.J. (2000) Incorporation of the nuclear pore basket protein nup153 into nuclear pore structures is dependent upon lamina assembly: evidence from cell-free extracts of Xenopus eggs. EMBO J. 19: 3918–3931

Starr, D.A., Fridolfsson, H.N. (2010) Interactions between nuclei and the cytoskeleton are mediated by SUN-KASH nuclear-envelope bridges. Annu. Rev. Cell Dev. Biol. 26: 421–444

Sugimoto-Shirasu, K., Stacey, N., Corsar, J. (2002) DNA Topoisomerase VI Is Essential for Endoreduplication in Arabidopsis. Curr. Biol. 12: 1782–1786

Sugimoto-Shirasu, K., Roberts, K. (2003) “Big it up”: endoreduplication and cell-size control in plants. Curr. Opin. Plant Biol. 6: 544–553

Sugimoto-Shirasu, K., Roberts, G.R., Stacey, N.J., McCann, M.C., Maxwell, A., Roberts, K. (2005) RHL1 is an essential component of the plant DNA topoisomerase VI complex and is required for ploidy-dependent cell growth. Proc. Natl. Acad. Sci. USA. 102: 18736–18741

Sullivan, T., Escalante-Alcalde, D., Bhatt, H., Anver, M., Bhat, N., Nagashima, K.et al. (1999) Loss of A-type lamin expression compromises nuclear envelope integrity leading to muscular dystrophy. J. Cell Biol. 147: 913–920

Swedlow, J.R., Sedat, J.W., Agard, D.A. (1997). Deconvolution in Optical Microscopy. *New York: Academic Press.*

Tamura, K., Fukao, Y., Iwamoto, M., Haraguchi, T., Hara-Nishimura, I. (2010) Identification and characterization of nuclear pore complex components in Arabidopsis thaliana. Plant Cell 22: 4084–4097

Tamura, K., Hara-Nishimura, I. (2011) Involvement of the nuclear pore complex in morphology of the plant nucleus. Nucleus 2: 168–172

Tamura, K., Iwabuchi, K., Fukao, Y., Kondo, M., Okamoto, K., Yeda, H., Nishimura, M., Hara-Nishimura, I. (2013) Myosin XI-i Links the Nuclear Membrane to the Cytoskeleton to Control Nuclear Movement and Shape in Arabidopsis Curr. Boil. In press

Tsien R.Y. (1998) The green fluorescent protein. Annu Rev Biochem. 67: 509-544

Tokuyasu, K. (1974) Dynamics of spermiogenesis in Drosophila melanogaster: IV. Nuclear transformation. J. Struct. Biol. 48: 284–303

Xu, X.M., Meulia, T., Meier, I. (2007) Anchorage of plant RanGAP to the nuclear envelope involves novel nuclear-pore-associated proteins. Curr. Biol. 17(13):1157-1163.

Yamada, K., Fukao, Y., Hayashi, M., Fukazawa, M., Suzuki, I., Nishimura, M. (2007) Cytosolic HSP90 regulates the heat shock response that is responsible for heat acclimation in Arabidopsis thaliana. J Biol Chem. 282(52):37794-3804.

Yang, L., Guan, T., Gerace, L. (1997) Integral membrane proteins of the nuclear envelope are dispersed throughout the endoplasmic reticulum during mitosis. J. Cell Biol. 137: 1199–1210

Yu, W., Moreno Díaz de la Espina, S. (1999) The plant nucleoskeleton: ultrastructural organization and identification of NuMA homologues in the nuclear matrix and mitotic spindle of plant cells. Exp. Cell Res. 246: 516–526

Zhao, Q., Brkljacic, J., Meier, I. (2008) Two Distinct Interacting Classes of Nuclear Envelope–Associated Coiled-Coil Proteins Are Required for the Tissue-Specific Nuclear Envelope Targeting of Arabidopsis RanGAP. Plant Cell 20: 1639–1651

Zhou, L., Panté, N. (2010) The nucleoporin Nup153 maintains nuclear envelope architecture and is required for cell migration in tumor cells. FEBS Lett. 584: 3013–3020

Zhou, X., Graumann, K., David, E.E., Iris, M. (2012) Novel plant SUN–KASH bridges are involved in RanGAP anchoring and nuclear shape determination. J. Cell Biol. 196: 203–211

Zirbel, R.M., Mathieu, U.R., Kurz, A., Cremer, T., Lichter, P. (1993) Evidence for a nuclear compartment of transcription and splicing located at chromosome domain boundaries. Chromosome Res. 1: 93-106